Ore Geology Reviews 86 (2017) 172–195

Contents lists available at ScienceDirect

Ore Geology Reviews

journal homepage: www.elsevier.com/locate/oregeo

Magmatic hydrothermal origin of the Hadamengou-Liubagou Au-Mo deposit, Inner Mongolia, China: Constrains on geology, stable and Re-Os isotopes

Yong-Mei Zhang [a], Xue-Xiang Gu [a,*], Zhong-Lin Xiang [b], Rui-Ping Liu [c], Wen-Bin Cheng [d], Xin-Li Wang [e]

[a] State Key Laboratory of Geological Processes and Mineral Resources, China University of Geosciences, Xueyuan Road 29, Beijing 100083, China
[b] Institute of Resources and Environment, Henan Polytechnic University, Jiaozuo 454000, China
[c] Beijing Research Institute of Uranium Geology, Beijing 100029, China
[d] College of Earth Sciences, Chengdu University of Technology, Chengdu 610059, China
[e] Xinda Gold & Silver Development Centre, Beijing 100038, China

ARTICLE INFO

Article history:
Received 29 August 2016
Received in revised form 25 January 2017
Accepted 30 January 2017
Available online 16 February 2017

Keywords:
Stable isotopes
Re-Os
Ore genesis
Hadamengou-Liubagou Au-Mo deposit
Inner Mongolia

ABSTRACT

The Hadamengou-Liubagou Au-Mo deposit is the largest gold deposit in Inner Mongolia of North China. It is hosted by amphibolite to granulite facies metamorphic rocks of the Archean Wulashan Group. To the west and north of the deposit, there occur three alkaline intrusions, including the Devonian-Carboniferous Dahuabei granitoid batholith, the Triassic Shadegai granite and the Xishadegai porphyritic granite with molybdenum mineralization. Over one hundred subparallel, sheet-like ore veins are confined to the nearly EW-trending faults in the deposit. They typically dip 40° to 80° to the south, with strike lengths from hundreds to thousands of meters. Wall rock alterations include potassic, phyllic, and propylitic alteration. Four distinct mineralization stages were identified at the deposit, including K-feldspar-quartz-molybdenite stage (I), quartz-pyrite-epidote/chlorite stage (II), quartz-polymetallic sulfide-gold stage (III), and carbonate-sulfate-quartz stage (IV). Gold precipitated mainly during stage III, while Mo mineralization occurred predominantly in stage I. The δD_{H2O} and $\delta^{18}O_{H2O}$ values of the ore-forming fluids range from −125‰ to −62‰ and from 1.4‰ to 7.5‰, respectively, indicating that the fluids were dominated by magmatic water with a minor contribution of meteoric water. The $\delta^{13}C_{PDB}$ and $\delta^{18}O_{SMOW}$ values of hydrothermal carbonate minerals vary from −10.3‰ to −3.2‰ and from 3.7‰ to 15.3‰, respectively, suggesting a magmatic carbon origin. The $\delta^{34}S_{CDT}$ values of sulfides from the ores vary from −21.7‰ to 5.4‰ and are typically negative (mostly −20‰ to 0‰). The wide variation of the $\delta^{34}S_{CDT}$ values, the relatively uniform $\delta^{13}C$ values of carbonates (typically −5.5‰ to −3.2‰), as well as the common association of barite with sulfides suggest that the minerals were precipitated under relatively high fo_2 conditions, probably in a magmatic fluid with $\delta^{34}S_{\Sigma S} \approx 0$‰. The Re-Os isotopic dating on molybdenite from Hadamengou yielded a weighted average age of 381.6 ± 4.3 Ma, indicating that the Mo mineralization occurred in Late Devonian. Collectively, previous ^{40}Ar-^{39}Ar and Re-Os isotopic dates roughly outlined two ranges of mineralizing events of 382–323 Ma and 240–218 Ma that correspond to the Variscan and the Indosinian epochs, respectively. The Variscan event is approximately consistent with the Mo mineralization at Hadamengou-Liubagou and the emplacement of the Dahuabei Batholith, whereas the Indosinian event roughly corresponds to the possible peak Au mineralization of the Hadamengou-Liubagou deposit, as well as the magmatic activity and associated Mo mineralization at Xishadegai and Shadegai. Geologic, petrographic and isotopic evidence presented in this study suggest that both gold and molybdenum mineralization at Hadamengou-Liubagou is of magmatic hydrothermal origin. The molybdenum mineralization is suggested to be associated with the magmatic activity during the southward subduction of the Paleo-Asian Ocean beneath the North China Craton (NCC) in Late Devonian. The gold mineralization is most probably related to the magma-derived hydrothermal fluids during the post-collisional extension in Triassic, after the final suturing between the Siberian and NCC in Late Permian.

* Corresponding author.
E-mail address: xuexiang_gu@cugb.edu.cn (X.-X. Gu).

http://dx.doi.org/10.1016/j.oregeorev.2017.01.029
0169-1368/

1. Introduction

The well-known Central Asian Metallogenic Domain (CAMD), extends from the Urals in the west, through Kazakhstan, Kyrgyzstan, northwestern China, Mongolia, southern Siberia, and northeastern China to the Pacific Ocean along the northwestern coast (Seltmann and Porter, 2005; Seltmann et al., 2014; Xue et al., 2016). It hosts numerous giant and world-class Cu-Au/Mo deposits, e.g., Oyu Tolgoi, Kounrad, Aktogai, and Almalyk that occur in Mongolia, Kazakhstan, and Uzbekistan (Fig. 1). The northern margin of the North China Craton (NCC), located in the mideast of the CAMD, is one of the most important metallogenic belts. Endowed with approximately 900 gold deposits, and dozens of molybdenum deposits, it becomes the second largest gold-producing base and the third largest molybdenum ore belt in China (Nie, 1997; Hart et al., 2002). Some of these deposits have genetic relationship with granitic intrusions (Nie, 1997; Hart et al., 2002; Yang et al., 2003). The Hadamengou-Liubagou Au-Mo deposit, located approximately 20 km west of Baotou city, is the largest gold deposit in Inner Mongolia. The deposit consists of the Hadamengou and Liubagou ore blocks with distance of 8 km, and is a unique example for a deposit containing both gold and molybdenum ores worldwide. Orebodies are spatially and genetically characterized by intensive alkali feldspar metasomatism, although phyllic alteration is common. Since 1986, hundreds of auriferous quartz veins and potassic-altered and silicified rocks have been sequentially discovered and the gold reserve reaches 170 tons nowadays (GHCAPF, 2011; Wang, 2016). Meantime, more and more molybdenum ores coexisting with gold were explored, although the present proved Mo reserve is only about 4600 t (GHCAPF, 2011).

Compared to the significant progress on ore prospecting in the deep and peripheral areas of the Hadamengou-Liubagou ore deposit, the scientific research work on this unique deposit is still limited. There are few detailed descriptions regarding spatial and temporal aspects of alteration and mineralization. The nature and origin of the hydrothermal fluids related to mineralization are poorly understood. In particular, there remains much controversy as to the ore genesis, including metamorphism, migmatitization, pegmatitic, and magmatic origins (Guo, 1992; Gan et al., 1994; GHCAPF, 1995; Chen et al., 1996; Nie et al., 2005). The relationship between gold and molybdenum mineralization is yet unclear. The major purposes of this paper are (1) to document in detail the geologic characteristics of the deposit, with an emphasis on the sequence and characteristics of mineral assemblages in different hydrothermal alteration and mineralization stages; (2) to present new data of stable (H, O, C and S) and Re-Os isotopes, in order to understand the source of ore-forming fluids and sulfur, as well as the timing of Mo mineralization; and (3) to classify the deposit type and address the temporal relationship issue between Au and Mo mineralization.

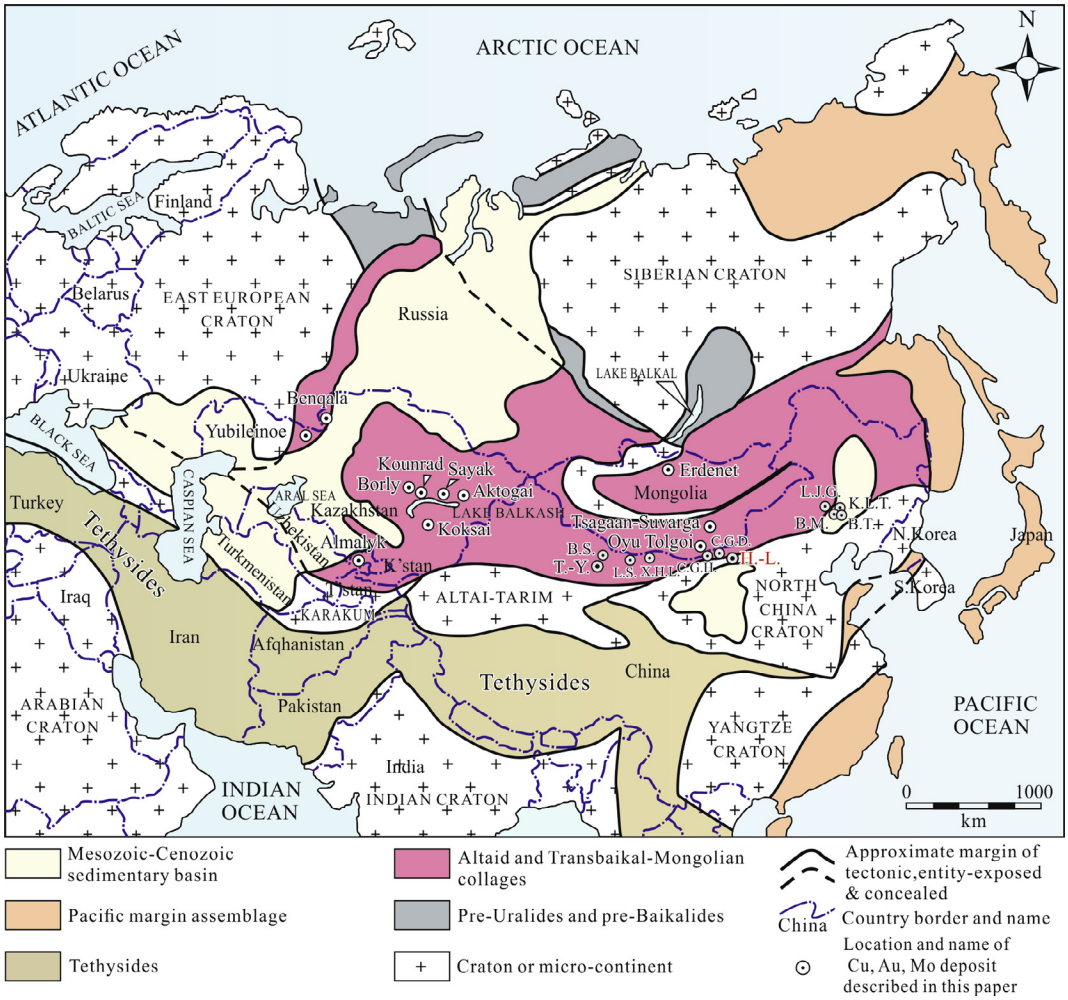

Fig. 1. Simplified tectonic location of the Central Asia Metallogenic Domain showing the distribution of major Cu-Au/Mo deposits associated with intermediate to felsic intrusions (modified after Seltmann et al., 2014). Abbreviations of deposits in China: Baimashi = B.M., Baituyingzi = B.T., Chagandeersi = C.G.D., Chaganhua = C.G.H., H.-L. = Hadamengou-Liubagou area (including Xishadegai Mo deposit), Kulitu = K.L.T., Laojiagou = L.J.G, Liushashan = L.S., Xiaohulishan = X.H.L., T.-Y. = Tuwu-Yandong.

The geological characteristics described in this paper indicate that the Hadamengou-Liubagou Au-Mo deposit is not of migmatitization or pegmatitic origin as previous studies (Gan et al., 1994; GHCAPF, 1995). Although present data of the deposit are partly consistent with that from both intrusion-related and orogenic gold deposits globally, they don't fit either existing genetic model well. The primary conclusion is that both molybdenum and gold mineralization is of magmatic hydrothermal origin. The Mo mineralization in the Hadamengou-Liubagou deposit is earlier than Au mineralization, rather than simultaneous or even later as Hou et al. (2011) proposed. A clearer link between the Au-Mo mineralization and protracted magmatic events are outlined than previous research (Guo, 1992; GHCAPF, 1995; Nie et al., 2005). The Au-Mo mineralization is coincident with episodic tectonic reactivations and associated magmatism in the region. Namely, the Variscan magmatic event is related to the Mo mineralization at Hadamengou-Liubagou. The Indosinian magmatism is suggested to be responsible for both the gold mineralization in the Hadamengou-Liubagou deposit and the Mo mineralization at Xishadegai.

2. Regional and deposit geology

The northern margin of NCC forms an EW-striking linear belt extending for almost 1500 km, from west of Baotou City across Inner Mongolia, northern Hebei province, north of Beijing and through Liaoning to southern Jilin province (Hart et al., 2002; Yang et al., 2003). There are mainly six gold ore clusters hosted in an uplifted Precambrian metamorphic basement (Fig. 2A). The Hadamengou-Liubagou Au-Mo deposit lying in the Late Archean basement belongs to the Wulashan-Daqingsha (I) ore cluster. It consists of the Hadamengou and the Liubagou ore blocks, and sandwiched between the Baotou-Hohhot Fault in the south and the Linhe-Jining Fault in the north, and is spatially associated with Phanerozoic granitic intrusions (Fig. 2B).

2.1. Basement rocks and structural framework

Amphibolite to granulite facies metamorphic rocks of the Archean Wulashan Group are the host rocks of the Hadamengou-Liubagou deposit. It is approximately 4 km thick and can be divided into three lithologic units from bottom to top (GHCAPF, 1995). The lower unit is largely composed of gneiss, amphibolite and granulite intercalated with magnetite quartzite and locally, migmatite. The middle unit mainly comprises gneiss, quartzite, leptite and thin layers of marble. The upper unit chiefly consists of gneiss, banded iron formation (BIF), quartzite and marble. Polycyclic sequences of amphibolite-gneiss-leptite-granulite, with original rocks varying from basalt/basaltic andesite through intermediate-acidic volcanic rocks to sedimentary rocks, suggest that the Wulashan Group may undergo multiple volcanic-sedimentary cycles.

Orebodies of the Hadamengou-Liubagou Au-Mo deposit are controlled by a series of subparallel, NWW-striking faults that are considered to be branch faults of the Baotou-Hohhot Fault, which in turn belongs to the Wulashan-Daqingshan Fault belt with striking NWW with a length of ~370 km from west of Urad Front Banner across Baotou City to Hohhot of Inner Mongolia. Geophysical data show that this fault belt may reach the Moho discontinuity and is thought to have existed since Late Archean and repeatedly activated until nowadays (GHCAPF, 1995). Tectonic evidence implies that its eastward extending Fengning-Longhua Fault is a reworked south-vergent thrust fault belt formed since Late Paleozoic (Zhang et al., 2004; Li, C.M. et al., 2016). A series of EW-, NW- and NE-trending subsidiary faults and fractures of this belt are considered to have controlled the Au-Mo mineralization in the Wulashan-Daqingshan area.

2.2. Intrusions

Magmatic activities were frequent and well developed in the study area. Batholiths, stocks and dikes are widespread in the metamorphic rocks of the Wulashan Group. There are three alkaline intrusions and hundreds of mafic to felsic dikes in the vicinity of the Hadamengou-Liubagou Au-Mo deposit (Fig. 2B).

The Dahuabei Batholith, with an outcrop area of approximately 180 km^2, is the largest intrusion in this district. It is located to the west of the Hadamengou-Liubagou ore deposit. The Batholith consists mainly of medium- to coarse-grained granite in central facies and medium- to fine-grained K-feldspar granite in marginal facies. U-Pb dating of zircon gave ages of 365.5 ± 7.3 Ma, 353 ± 7 Ma and 330 ± 10 Ma, suggesting its emplacement in the Variscan epoch (Miao et al., 2000; Li et al., 2009; Zhang, 2012).

The Xishadegai stock, located ~1.5 km to the northeast of the Dahuabei Batholith, is host to the Xishadegai medium-sized Mo deposit. With an irregular shape and an outcrop area of 11 km^2, the stock is mainly composed of medium- to coarse-grained porphyritic granite and medium- to fine-grained porphyritic moyite with zircon U-Pb age of 232.7 ± 4.1 Ma (Sun, 2016). Re-Os dating of the molybdenite ore at Xishadegai yielded an isochron age of 225.4 ± 2.6 Ma (Zhang et al., 2011a).

The Shadegai intrusion, adjacent to the Xishadegai deposit, occurs as an irregular stock with an outcrop area of 65 km^2. It consists mainly of medium- to coarse-grained biotite moyite with abundant microgranular enclaves of monzonite. Zircon U-Pb isotopic dating of moyite and monzonite at Shadegai using laser ablation-inductively coupled plasma-mass spectrometry (LA-ICP-MS) gave similar ages of 233.4 ± 2.3 Ma and 229.7 ± 1.5 Ma, respectively (Gu et al., 2015). Both the Xishadegai and the Shadegai granites formed during the Indosinian epoch. Geochemically, the three intrusions are predominantly alkaline, metaluminous to weakly peraluminous, and highly fractionated I-type felsic rocks (Zhang, 2012). The magmas were moderately oxidized and contain significant crustal components (Zhang, 2012).

A great number of predominantly EW-trending granitic pegmatite and diabase dikes occur in the Wulashan Group metamorphic rocks, ranging in width from 1 to 18 m and length from several meters to a few kilometers. They are considered to be genetically related to the gold mineralization at Hadamengou by some early researchers (GHCAPF, 1995). Six zircon U-Pb ages of different pegmatite dikes outlined an age range of 1981–1821 Ma (Zou et al., 1998; Miao et al., 2000; Zhang, 2012), that corresponds to the syn- to post-orogeny of the Late Paleoproterozoic Lvliang Movement in North China. Diabase dikes are usually several to several hundred meters long, with width from 5 to 50 m. Two dikes of EW- and NS-striking yielded zircon U-Pb ages of 1773 ± 11 Ma and 1785 ± 14 Ma, respectively (Wang, 2016).

2.3. General features of ore deposit

The Hadamengou-Liubagou ore deposit comprises over one hundred gold-bearing veins that locally also contain molybdenum. These ore veins have similar geological characteristics and are distributed in adjacent exploration areas named Hadamengou and Liubagou ore blocks which are about 8 km apart (Fig. 2B). The Hadamengou (also known as Wulashan) ore block was discovered in 1986 (GHCAPF, 1995). It is mainly composed of No. 13, 24, 49, 1, 59 and 113 vein clusters with totally more than 90 veins (Fig. 2B). The Liubagou ore block, discovered in 1991 (GHCAPF, 1995), consists mainly of No. 313, 314 and 307 veins (Fig. 2B). Most of these ore veins are confined to the nearly EW-trending faults and locally

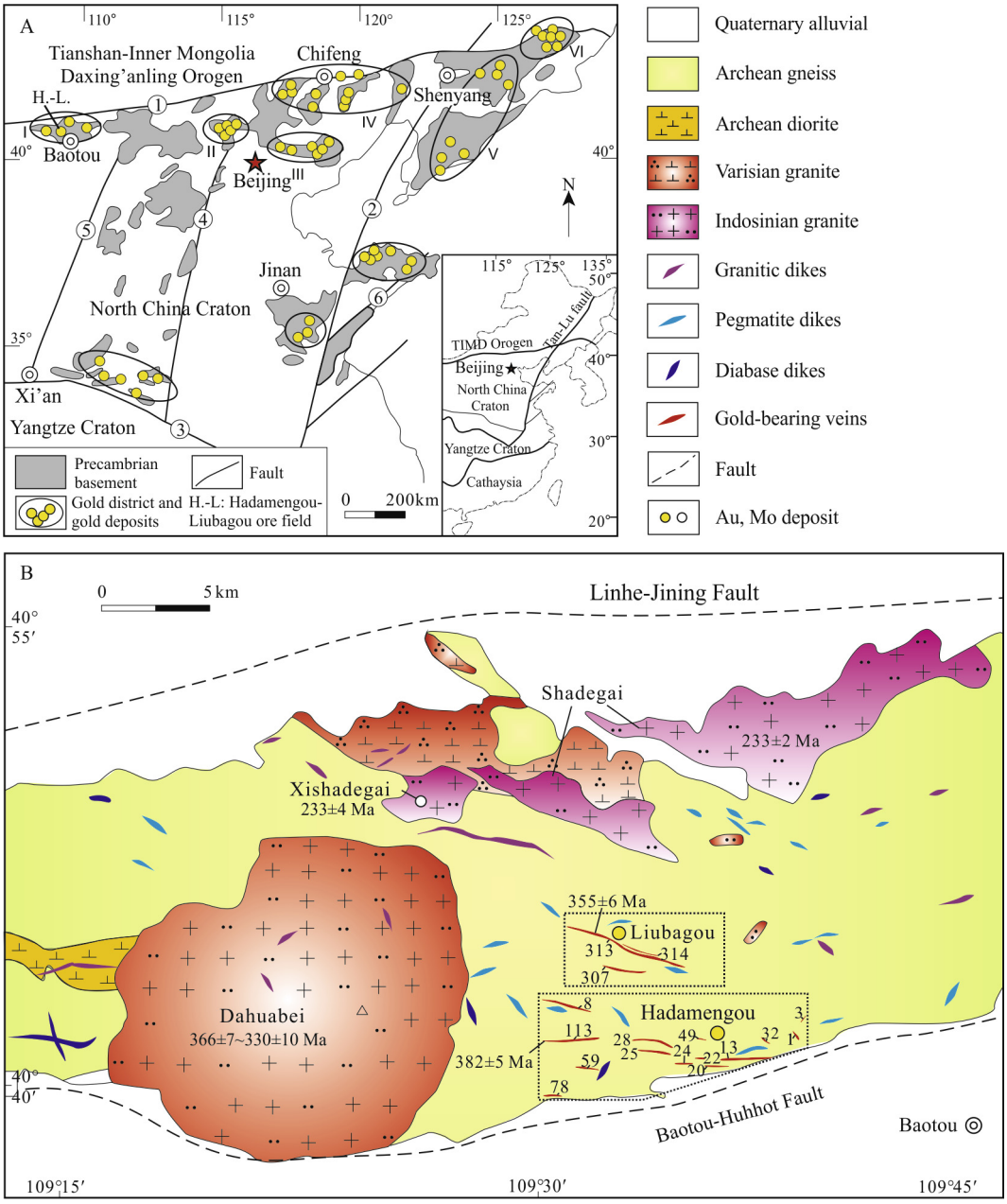

Fig. 2. Skech maps showing the distribution of gold deposits in the north margin of North China Craton (A, after Yang et al., 2003) and the geology of the Wulashan area (B, after Zhang, 2012). Gold districts: (I) Daqingshan-Wulashan; (II) Zhang-Xuan; (III) eastern Hebei-western Liaoning; (IV) Chifeng-Chaoyang; (V) eastern Liaoning; (VI) southern Jilin. Faults: ① Chifeng-Kaiyuan fault; ② Tan-Lu fault; ③ Xiaotian-Mozitan fault; ④ Xingyang-Kaifeng-Shijiangzhuang-Jianping fault; ⑤ Huashan-Lishi-Datong-Duolun fault; ⑥ Wulian-Mishan fault.

crosscut by the NE-trending faults. In this ore deposit, the veins of No.313 at Liubagou, as well as No.13 and No. 113 vein at Hadamengou account for most of the proven ore reserves and have been systematically explored by trenches, tunnels, and drills. Most samples analyzed in this study were collected from these veins considering spatial representation of samples.

The ore vein (orebody) No. 313 at Liubagou is mainly hosted in amphibole-gneiss and biotite-gneiss of the upper unit of the Wulashan Group. It confines to a NWW-striking fault and is crosscut and offset by a NE-trending fault (F_{302} in Fig. 3). The western-most point of this vein is about 5 km away from the eastern margin of the Dahuabei Batholith and the Xishadegai granite. It strikes approximately E and dips 40° to 70° to the south. The ore vein is typically sheet-like, with a strike length of ~5800 m, a dip extent up to ~1200 m (generally 800–1000 m), and a true thickness ranging from 0.8 to 18.4 m (average of 3.3 m). The proven reserves comprise nearly 70 t Au and over 4600 t Mo, with Au grades ranging from 0.8 to 22.6 ppm (average of 2.26 ppm) and an average Mo grade of 0.048% (GHCAPF, 2011). Ore mainly occurs as auriferous quartz veins, Au-bearing potassic-altered and silicified rocks with disseminated pyrite, and locally breccias (Fig. 4).

The ore vein No. 13 at Hadamengou is localized within garnet-biotite gneiss and biotite-gneiss of the middle and lower unit of the Wulashan Group. It is located about 13 km away from the eastern margin of the Dahuabei Batholith. The orebody strikes E and dips 45° to 80° to the south, with a strike length of ~2200 m, a dip extent of 1100 m, and a true thickness varying from 0.2 to 9.7 m (average of 2.3 m). The proven gold reserve is around 25 t, with

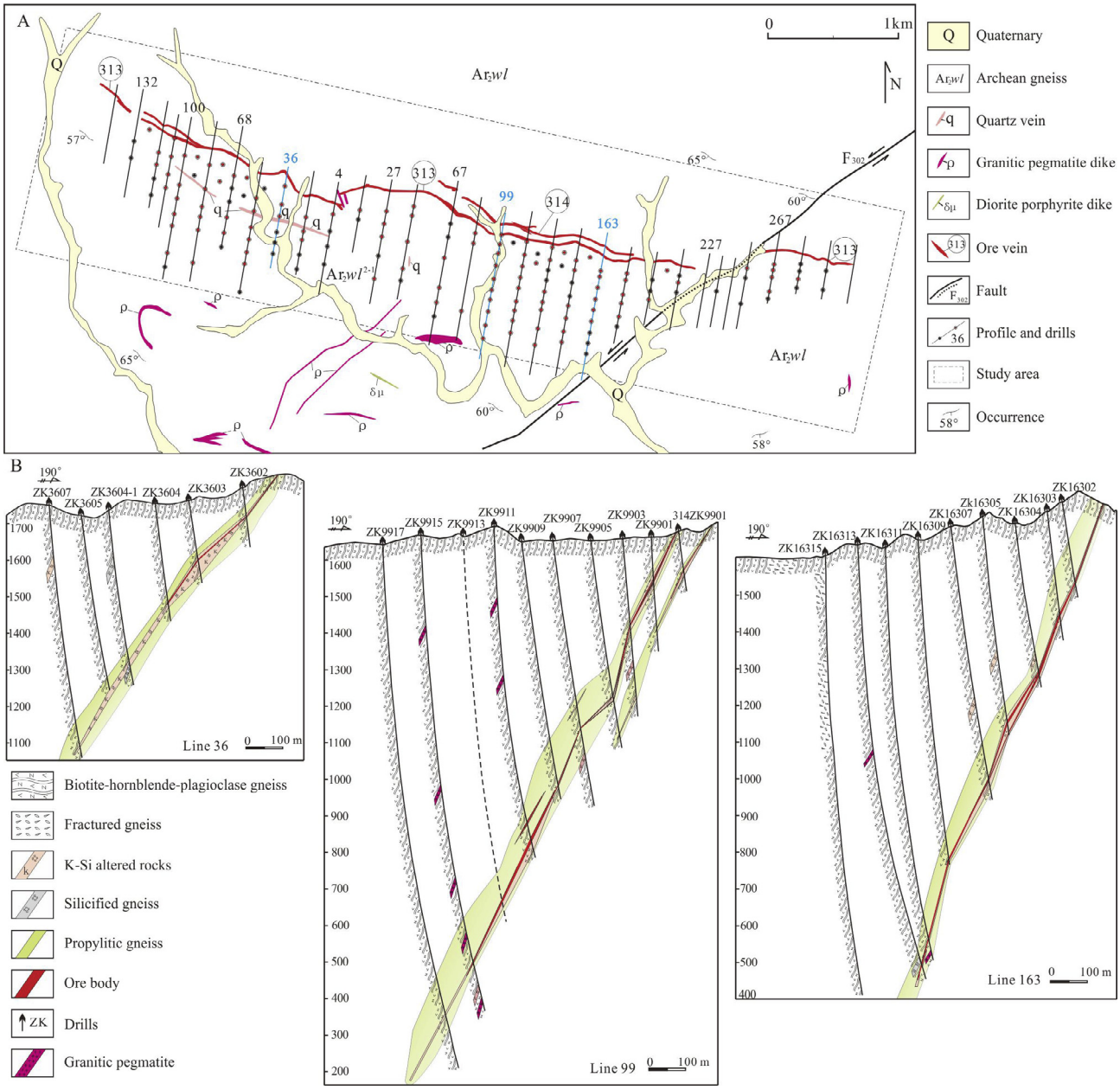

Fig. 3. Geologic map (A) and typical prospecting profiles (B) of the Liubagou Au-Mo ore block.

Au grades ranging from 0.8 to 83 ppm (average of 3.6 ppm) (GHCAPF, 1995, 2011). Molybdenum mineralization associated with gold occurs locally in the deep part of the vein.

The ore vein No. 113 is situated at the west segment of the Hadamengou ore block. Its western-most point is approximately 5 km away from the eastern margin of the Dahuabei Batholith. It strikes ENE to ESE and dips 43° to 74° to the south, with a strike length of 3040 m, a dip extent of ~900 m, and a true thickness ranging from 0.4 m to 5.3 m (average of 1.8 m). The proven Au reserve is about 4 t with grades of 1.1–9.4 ppm (average 3.2 ppm) (GHCAPF, 1995, 2011). Molybdenum mineralization occurs locally and the Mo grades range from 0.03% to 0.20% with a mean of 0.046% (GHCAPF, 2011).

3. Sampling and methods

Field data and the studied samples were collected from outcrops, trenches, tunnels, and over 100 drill cores in the Hadamengou-Liubagou ore deposit. Three vertical sections at Liubagou were selected for detailed study (Fig. 3B). For comparison, a few samples were collected from the Hadamengou ore block.

Paragenetic study was based on field observations as well as on hand specimens and microscopic petrography. About 370 thin sections were studied under transmitted and reflected light microscope. Scanning electron microscope with energy dispersive spectrometry (SEM-EDS) was used to aid mineral identification, each accompanied by a back-scattered electron (BSE) image in Western Washington University.

Hydrogen and oxygen isotopes of fluid inclusions hosted in K-feldspar and quartz were analyzed using a Finnigan MAT253-type mass spectrometer at the Stable Isotope Laboratory of Mineral Resources Institute in Beijing, Chinese Academy of Geological Sciences, following the method of Clayton and Mayeda (1963). Oxygen gas was produced by quantitatively reacting the samples with BrF_5 in externally heated nickel reaction vessels. Hydrogen was determined by quantitatively reacting the H_2O with zinc at

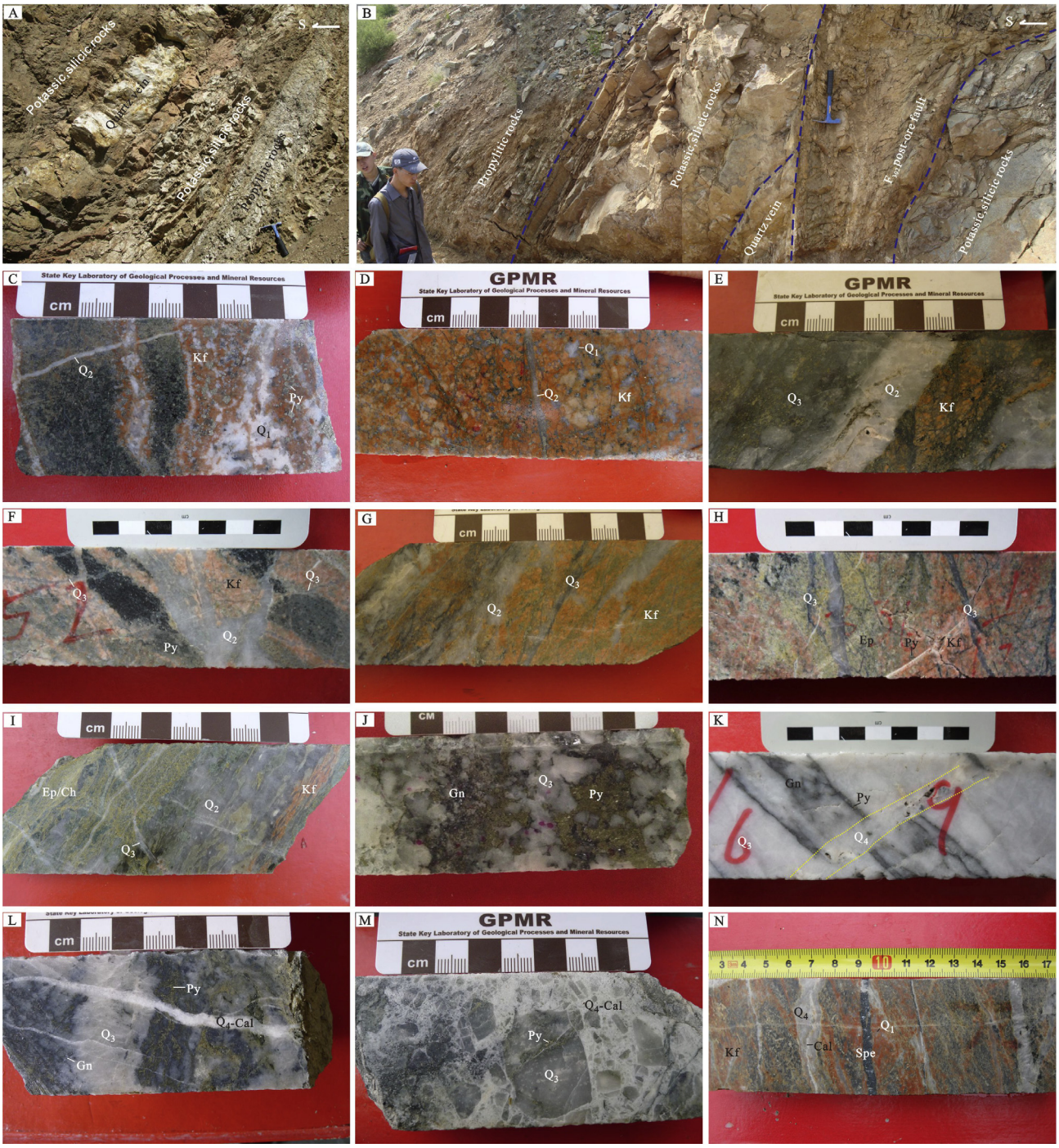

Fig. 4. Alteration, mineral assemblage and crosscutting relationships of different hydrothermal stages in the Hadamengou-Liubagou Au-Mo deposit. A. Zonation of alteration in the Liubagou ore block. Orebodies consist of quartz vein and potassic, silicified rocks. Propylitization and carbonatization develop adjacent to orebodies. B. Orebodies and altered rocks are controlled by EW-trending fault and destructed by the NE-trending F_{302} fault. C, D. K-feldspar and wavy quartz (Q_1) of stage I cut by quartz veinlets of stage II (Q_2). E. Potassic altered rocks cut by quartz veins of Stage II and stage III (Q_2, Q_3). F, G. Early stage potassic-silicified rocks with disseminated pyrite cut by quartz veinlets of stages II and III (Q_2, Q_3). H, I. Stage I potassic rocks overprinted by stage II quartz (Q_2) -epidote-chlorite. Smoky quartz veinlets of stage III (Q_3) cut both stage I and stage II mineral assemblages. J. Stage III quartz (Q_3) intergrown with pyrite and galena. K, L. Stage III quartz (Q_3)-sulfide vein cut and displaced by milky quartz (Q_4)-calcite veinlets of stage IV. M. Smoky quartz of stage III (Q_3) fractured and cemented by calcite-quartz (Q_4) veinlets of stage IV. N. Quartz, calcite and specularite veinlets of stage IV cut stage I potassic-silicified rocks. Mineral abbreviations are the same as footnotes in Table 1.

temperature of 550 °C. The results adopted the Standard Mean Ocean Water (SMOW) as standards, with a precision of ±2‰ for δD and ±0.2‰ for $\delta^{18}O$.

Sulfur and carbon-oxygen isotopic compositions for hydrothermal sulfides and carbonates were determined at the Analytical Laboratory of Beijing Research Institute of Uranium Geology. Sulfide samples were converted into SO_2 for S isotopic analyses by quantitatively oxidation reacting with Cu_2O. The $\delta^{34}S$ values were measured using a Finnigan MAT 251 mass spectrometer with respect to the Canyon Diablo Troilite (CDT) standard. CO_2 for C-O isotopes was produced by quantitatively reacting carbonate samples with phosphoric acid at a temperature of 25 °C, and was analyzed by a Finnigan MAT 253 mass spectrometer. Results of the C and O isotopic analyses obtained where measure with respect to

the Pee Dee Belemnite (PDB) and SMOW, respectively. The accuracy for all data is better than ±0.2‰.

Eight molybdenite samples were collected from the gold-bearing quartz-molybdenite vein of the orebody No. 113 at Hadamengou. Gravitational and magnetic separations were applied and mineral grains were picked up under a binocular microscope with purity over 98%. Re-Os isotope analyses were performed using a TJA X-series ICP-MS in the Re-Os Laboratory, National Research Center of Geoanalysis, Chinese Academy of Geological Sciences in Beijing, following the procedures of Du et al. (2004). The GBW04435 (HLP) standard was used for quality control. Concordia diagrams and weighted mean calculations were made using Isoplot (Ludwig, 2004), where the decay constant of ^{187}Re adopted is 1.666×10^{-11} a^{-1}.

4. Results

4.1. Wall rock alterations and hydrothermal mineral assemblages

Wall rock alterations are widely developed in the Hadamengou-Liubagou ore deposit, including potassic, phyllic, and propylitic alteration. Potassic alteration is represented by a great deal of K-feldspar, minor biotite and albite. Phyllic alteration is characteristic of quartz veins, minor pyrite and sericite. Propylitic alteration mainly consists of chlorite, epidote, calcite, and pyrite. Zonation of alteration envelopes can be observed at both macro and micro scales. Quartz veins usually outcrop in the center of orebodies. Potassic and silicified rocks develop at both sides of quartz veins. Propylitic rocks occur at the outermost positions away from orebodies (Fig. 4A, B). Alteration zones transit gradually from the middle to both sides, and usually overlap with each other near transitional zones due to multi-episode of mineralization. In general, alteration is more intense and commonly thicker in the hanging-wall than in the footwall (Fig. 3).

Based on field crosscutting relationships and mineral paragenesis, four distinct stages of gold mineralization were identified at the Hadamengou-Liubagou ore deposit, including K-feldspar-quartz-molybdenite stage (I), quartz-pyrite-epidote/chlorite stage (II), quartz-polymetallic sulfide-gold stage (III), and carbonate-sulfate-quartz stage (IV). Gold precipitated mainly during stage III, and to a less extent during stages I and II, while Mo mineralization occurred mainly in stage I. Mineral assemblages of every stage are listed in Table 1 and illustrated in Figs. 4–7.

4.1.1. K-feldspar-quartz-molybdenite stage (I)

Mineral assemblage of this stage is spatially and genetically related to potassic alteration. Hydrothermal minerals include K-feldspar, quartz, molybdenite, magnetite, pyrite, and minor calcite, ankerite, dolomite, biotite, albite and barite. K-feldspar is pervasive in the altered gneiss, forming a 3–5 m wide pale red zone which is easily identified in field and recognized as an important indicator for ore prospecting. Quartz (Q_1) occurs as wavy or worm-like patches distributed in altered rocks (Fig. 4C, D). It is commonly intergrown with and locally enveloped by K-feldspar. Molybdenite typically occurs either as disseminates in potassic-altered and silicified rocks (Fig. 5A, B), or as deformed and fractured K-feldspar-biotite-pyrite-molybdenite-carbnate veinlets/aggregates which are cemented by quartz veins of stage II and/or stage III (Fig. 5C–E). Pyrite has relatively low relief and a poor polish. Carbonate minerals are commonly intergrown with K-feldspar and biotite, and locally replaced by later stage quartz (Fig. 5E). The mineral assemblage of this stage is usually fractured and cemented or crosscut by the minerals of later stages (II, III and IV, Figs. 4, and 5C–E).

4.1.2. Quartz-pyrite-epidote/chlorite stage (II)

The mineral assemblage including quartz, pyrite, epidote, chlorite and minor sericite is related to phyllic and propylitic alteration in this stage (Fig. 4D–I). Feldspar, biotite and magnetite are widely distributed in pale green rocks as relic minerals of gneiss. Milky to grey-white quartz (Q_2) either cuts the early stage potassic-altered and silicified rocks as veins and veinlets (Fig. 4E–G), or is pervasively distributed in propylitic rocks as irregurlar aggregates (Fig. 4I). Pyrite is medium to coarse grained, sub-euhedral to euheral and commonly intergrown with quartz. Epidote and chlorite usually develop along fractures or gneissosity on both sides of the earlier potassic, silicified rocks, forming a pale green zone of several meters to over ten meters in width. Gold was not observed in this stage, although low grade quartz-pyrite veins are locally recognized.

4.1.3. Quartz-polymetallic sulfide-gold stage (III)

Quartz-polymetallic sulfide veins of this main ore stage typically cut the earlier stage altered rocks and veins (Figs. 4F-I). Hydrothermal minerals of this stage include quartz, pyrite, galena, chalcopyrite, as well as minor gold, calaverite, altaite, sericite, apatite, dolomite, barite and celestine. At the upermost parts of the deposit, sulfides are locally oxidized to supergene minerals including covellite, malachite, cerussite and hematite. Quartz (Q_3) typically occurs as several centimeters to several meters wide smoky gray veins and contains abundant and various sulfides than those of stage II (Fig. 4E, J, and 6D, E). Pyrite is disseminated in quartz veins and locally intergrown with galena and chalcopyrite. It is fine-grained, subhedral to anhedral, and typically exhibits high relief and smooth polish under the microscope (Fig. 6B, F). Gold grains of irregular and round shapes either fill in fractures or included in pyrite and quartz, or less commonly, occur at the margin of dolomite (Fig. 6A–C). Microprobe analyses show that most of the gold has a high fineness ranging from 847 to 990 (GHCAPF, 1995; Zhang, 2012). A small amount of gold also occurs as calaverite (Fig. 6F), petzite, and electrum (GHCAPF, 1995). Barite and celestine associated with galena, pyrite and apatite were occasionally observed infilling fissures of quartz (Fig. 6E).

4.1.4. Carbonate-sulfate-quartz stage (IV)

The assemblage of carbonate, sulfate and quartz of this stage typically occurs as veins or veinlets cutting all veins of earlier

Table 1
Mineral assemblages of different stages in the Hadamengou-Liubagou Au-Mo deposit.

Stage	Non-metal minerals	Metal minerals	Relic minerals	Paragenetic relationship
I	Kf, Q, ± (Bi, Ank, Dol, Ab)	Py, Mot, ± (Mt)	Plag, Kf, Q, Hb, Bi, Ap	Cut by Q_2, Q_3, Q_4, Cal and Spe vein
II	Q, Ep, Ch, ± (Ser)	Py	Plag, Kf, Mt, Bi	Cut Kf and Q_1, cut by Q_3 vein
III	Q, ± (Dol, Ap, Ser, Brt, Cel)	Py, Cp, Gn, ± (Gl, Cav, Alt)	Bi, Zr, Mon, Rut, Mt	Cut Q_2, cut by Q_4 or cement by Cal
IV	Cal, Q, Brt, ± (Cel)	Spe, ± (Sid)		Cut all other vein types

Mineral abbreviations: Ab-Albite, Alt-altaite, Ank-ankerite, Ap-apatite, Brt-barite, Bi-biotite, Cal-calcite, Cav-calaverite, Cel-celestine, Ch-chlorite, Cp-chalcopyrite, Dol-dolomite, Ep-epidote, Gl-gold, Gn-galena, Hb-hornblende, Kf-K-feldspar, Mon-monazite, Mot-molybdenite, Mt-magnetite, Plag-plagioclase, Py-pyrite, Q-Quartz, Rut-rutile, Ser-sericite, Sid-siderite, Spe-specularite, Zr-zircon.

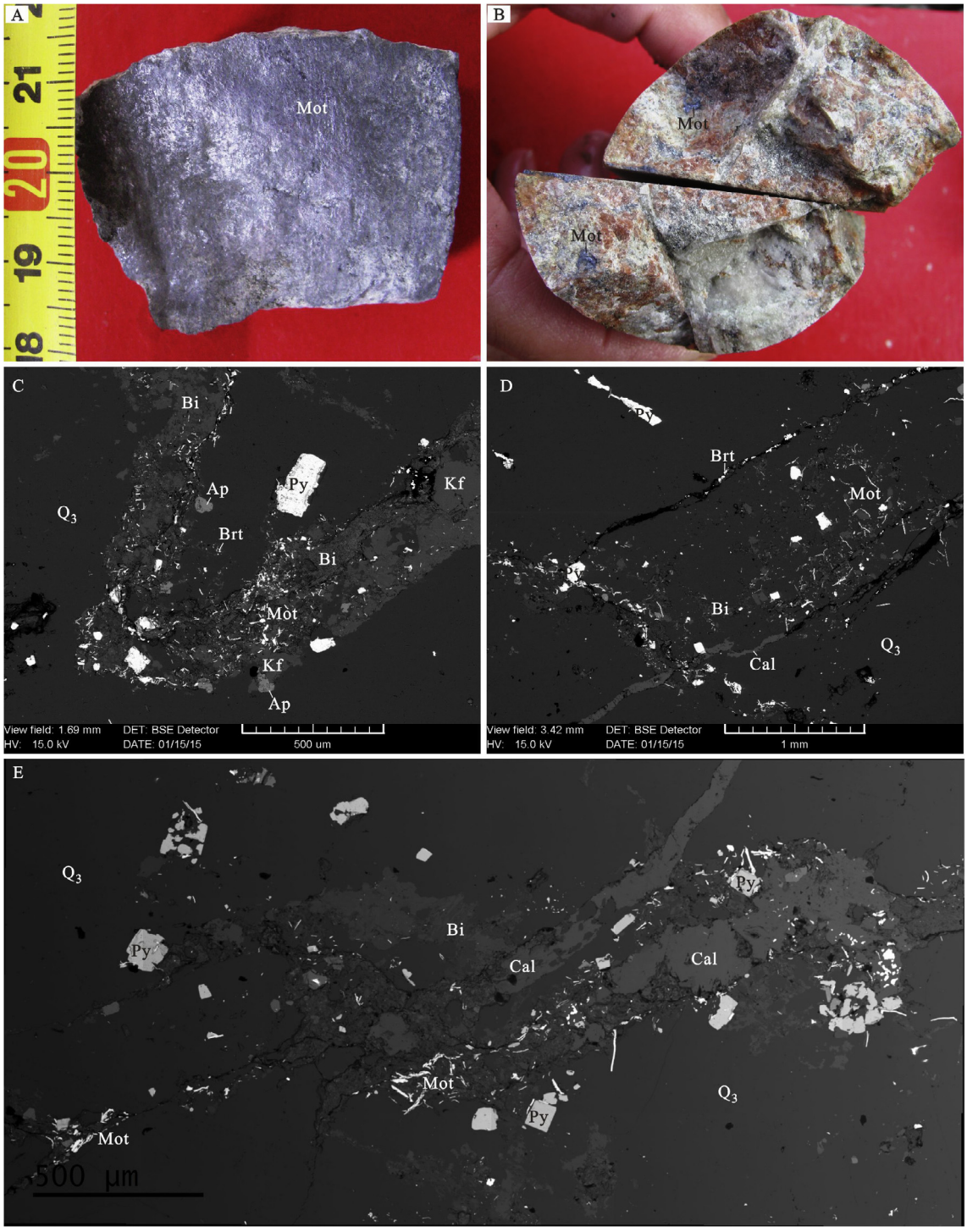

Fig. 5. Molybdenite occurrence on hand samples and under microscope in the Hadamengou-Liubagou Au-Mo deposit. A, B. Molybdenite disseminated in potassic, silicified altered rocks of stage I. C. Stage I molybdenite + pyrite + K-feldspar + biotite veinlets strongly deformed and enveloped by stage III quartz (Q_3). D. Molybdenite, pyrite and biotite of stage I replaced by stage III quartz (Q_3) which is in turn cut by calcite and barite veinlets of stage IV. E. Stage I K-feldspar-biotite-pyrite-molybdenite-carbonate veinlets partly replaced by stage III quartz (Q_3). Mineral abbreviations are the same as footnotes in Table 1. Microphotos C to E are BSE images.

stages (Figs. 4K–N and 6H). Carbonate veinlets locally containing minor barite and celestine are widespread in the entire altered rocks, infilling fractures and overprinting earlier mineralization stages (Fig. 6A, H). Quartz veins/veinlets (Q_4) are milky and of several millimeters to tens of centimeters wide, occasionally with vugs or overgrown by calcite in center (Fig. 4N). Specularite veinlets of millimeter- to centimeter-scale is also occasionally observed in the assemblage of this stage (Fig. 4N).

4.2. Hydrogen-oxygen isotopes

The hydrogen and oxygen isotopic data and calculated $\delta^{18}O_{H2O}$ values at Hadamengou-Liubagou are listed in Table 2 and illustrated in Fig. 8. Fifteen samples from ore vein No. 313 at Liubagou and five samples from ore vein No. 13 at Hadamengou were analyzed in this study on the fluid inclusions hosted in both K-feldspar and quartz of different stages. Eighteen data of fluid inclusions hosted

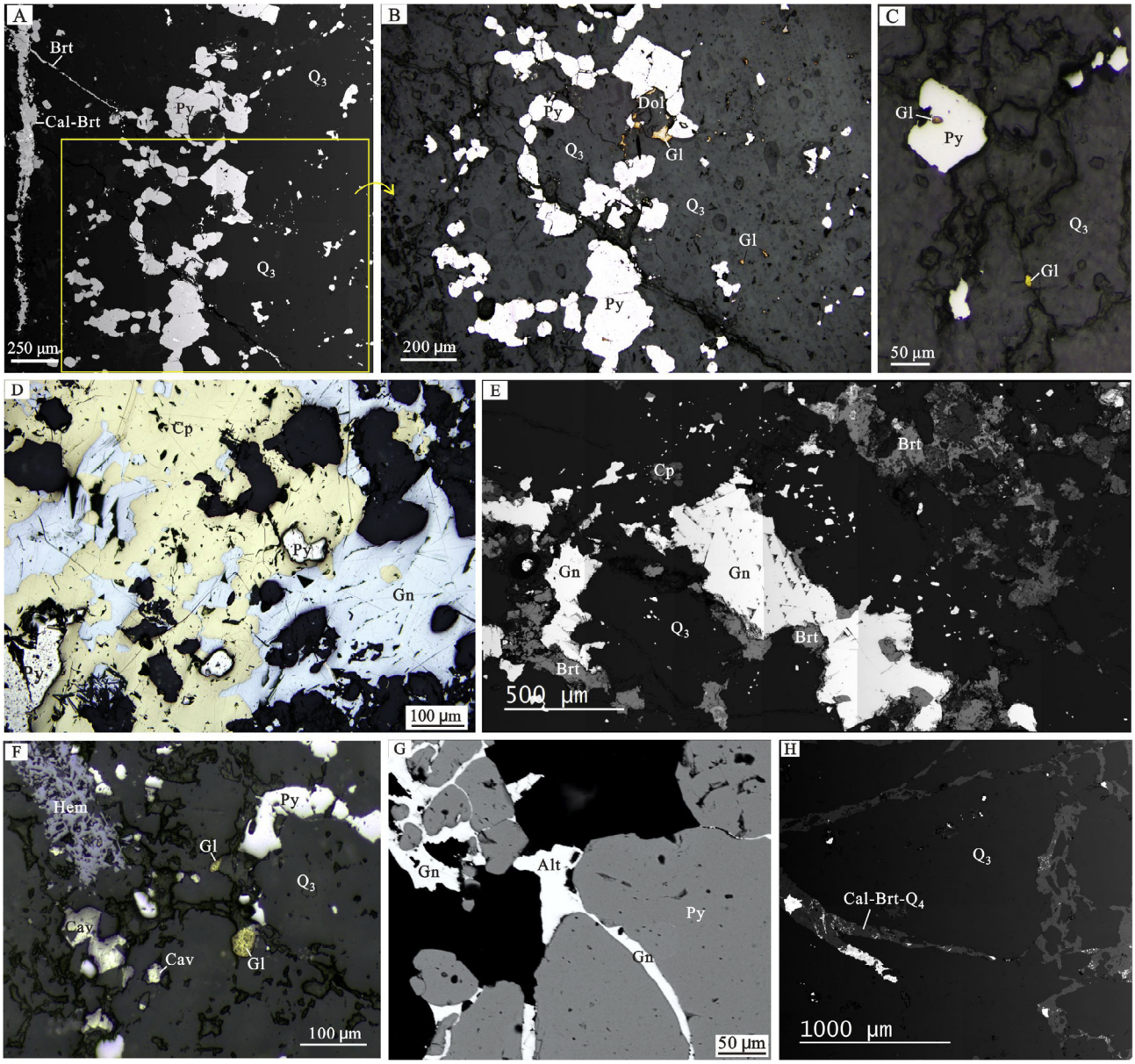

Fig. 6. Microphotos showing gold occurrence and mineral assemblages of different stages in the Hadamengou-Liubagou Au-Mo deposit. A-C. Gold grains intergrown with pyrite or as inclusions in pyrite and quartz of stage III. Calcite-barite veinlets of stage IV cut stage III quartz (Q_3). D. Early stage pyrite replaced by stage III chalcopyrite and galena. E. Stage III assemblage of quartz (Q_3), galena, chalcopyrite and barite. F. Gold, calaverite, and pyrite disseminated in stage III quartz. G. Galena and altaite of stage III fill in the fracture of stage II pyrite. H. Calcite-barite veinlets of stage IV fill in microfissures of stage III quartz. Mineral abbreviations are the same as footnotes in Table 1. Microphotos B, C, D, and F are taken under reflect light microscope. The others are BSE images.

in quartz from ore vein No. 13 and No. 313 at Hadamengou were collected from previous studies (Hou, 2011; Wang, 2016). The $\delta^{18}O_{H2O}$ values were calculated based on the fluid inclusion homogenization temperatures and fractionation equations between minerals and water (Clayton et al., 1972; Taylor, 1974).

In the Liubagou ore block, the $\delta^{18}O_{H2O}$ values of K-feldspar and quartz range from 1.4‰ to 6.1‰ (average 4.5‰), and the δD_{H2O} values vary between −125‰ and −80‰ (average −96‰). In the Hadamengou ore block, the $\delta^{18}O_{H2O}$ and δD_{H2O} values of the ore veins No. 13 and No. 113 range from 3.8‰ to 7.5‰ and from −103‰ to −62‰, respectively.

4.3. Carbon-oxygen isotopes

Carbon-oxygen isotopic compositions of carbonate and quartz in the Hadamengou-Liubagou deposit are presented in Table 3 and Fig. 9. Three samples from ore vein No. 313 at Liubagou were analyzed in this study, and seven data from ore vein No. 13 and No. 113 at Hadamengou were collected from GHCAPF (1995) and Xie (2011). The $\delta^{18}O_{SMOW}$ values were calculated using the formula of Friedman et al. (1977). In the Liubagou ore block, the $\delta^{13}C_{PDB}$ and $\delta^{18}O_{SMOW}$ values of three calcite samples range from -10.3‰ to -5.0‰ and from 7.3‰ to 15.3‰, respectively. In the Hadamengou ore block, the $\delta^{13}C_{PDB}$ and $\delta^{18}O_{SMOW}$ values of two ankerite samples vary from −5.1‰ to −4.0‰ and from 3.7‰ to 10.1‰, respectively; whereas those of two calcite samples are −3.2‰ and from 11.8‰ to 12.8‰, respectively GHCAPF (1995). The $\delta^{13}C_{PDB}$ and $\delta^{18}O_{SMOW}$ values of fluid inclusions hosted in quartz are similar to those of carbonates (Xie, 2011).

4.4. Sulfur isotopes

Eleven samples of sulfides including pyrite, galena and chalcopyrite from ore vein No. 313 were analyzed for sulfur isotopes

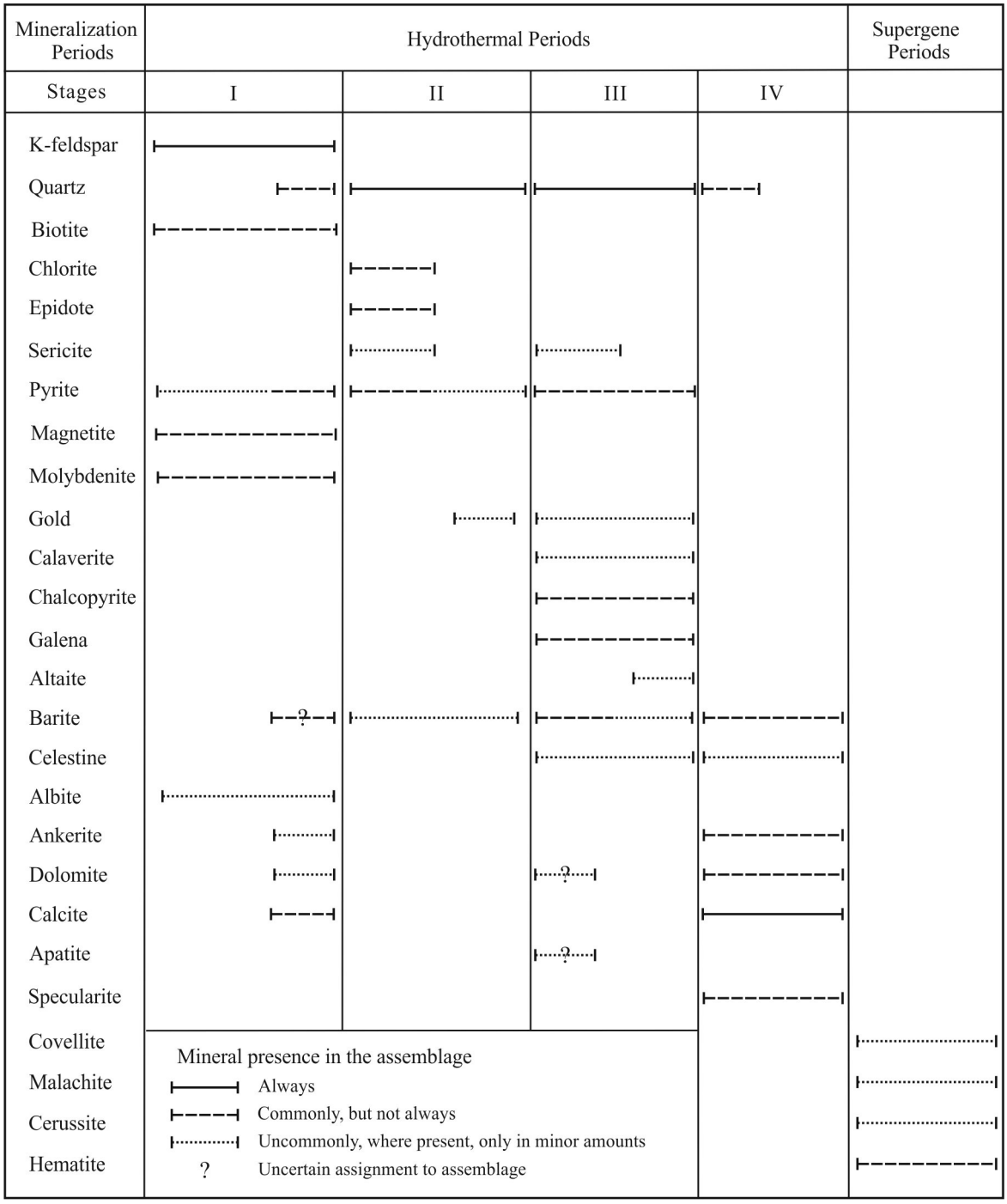

Fig. 7. Paragenetic sequence of ore, gangue, and alteration minerals in the Hadamengou-Liubagou Au-Mo deposit.

at Liubagou. Eighty sulfur isotopic data focusing on Hadamengou and Dahuabei Batholith were collected from previous studies (Guan et al., 1992; Nie and Bjorlykke, 1994; Lang and Li, 1998; Hou, 2011; Xie, 2011). The results are listed in Table 4 and illustrated in Fig. 10. The $\delta^{34}S_{CDT}$ values ($n = 15$) of sulfides from the ores at Liubagou range between −15.4‰ and −4.3‰ with an average of −11.4‰. Two pairs of coexisting pyrite and galena from same quartz ore show that $\delta^{34}S_{pyrite}$ values are greater than $\delta^{34}S_{galena}$ values. The $\delta^{34}S_{CDT}$ values of 72 sulfide samples from the Hadamengou ore block range widely from −21.7‰ to 5.4‰, typically between −20‰ and 0‰. Sulfur isotopes of galena ($n = 18$) cover the full range of data, whereas pyrite ($n = 49$) and chalcopyrite ($n = 5$) have $\delta^{34}S_{CDT}$ values from −18.4‰ to 2.0‰ and from −14.3‰ to 4.4‰, respectively. Three of four pyrite-galena pairs show larger $\delta^{34}S_{CDT}$ values in pyrite than in galena (Fig. 8). The $\delta^{34}S_{CDT}$ values of barite and celestite coexisting with galena are 6.1‰ and 4.3‰, respectively. The $\delta^{34}S_{CDT}$ values of two pyrites from the Dahuabei granite range from 1.3‰ to 2.0‰.

4.5. Rhenium-osmium dating

Results of Re-Os dating are listed in Table 5 and illustrated in Fig. 11. The concentrations of ^{187}Re and ^{187}Os range from 1.13 ppm to 6.42 ppm and from 7.1 ppb to 40.9 ppb, respectively.

Table 2
Hydrogen and oxygen isotopic compositions of hydrothermal minerals and fluids in the Hadamengou-Liubagou Au-Mo deposit.

Ore block	Vein No.	Sample No.	Mineral/stage	$\delta^{18}O_{SMOW}$/‰	δD_{H2O}/‰	$\delta^{18}O_{H2O}$/‰	T/°C	Data sources
Liubagou	313	313TK-5	K-feldspar/I	8.0	−96	4.8	393	This study
		PD1-2	K-feldspar/I	9.1	−125	5.7	393	
		ZK12303-7-2	K-feldspar/I	8.1	−100	4.7	393	
		ZK3603-7	Quartz/II	12.6	−94	4.7	273	
		ZK0402-11	Quartz/II	13.0	−80	5.1	273	
		ZK17903-6	Quartz/III	12.1	−102	4.1	271	
		ZK12402-3	Quartz/III	12.4	−99	4.4	271	
		PD2-5	Quartz/III	12.0	−89	4.0	271	
		ZK10802-4	Quartz/III	11.8	−84	3.8	271	
		ZK16304-16-1	Quartz/III	11.9	−96	3.9	271	
		ZK16305-28-2	Quartz/III	12.0	−102	4.0	271	
		ZK17905-15	Quartz/III	14.1	−96	6.1	271	
		ZK2004-10	Quartz/III	12.5	−84	4.5	271	
		ZK9903-14	Quartz/III	9.4	−96	1.4	271	
		313TK-10	Quartz/III	13.8	−98	5.8	271	
Hadamengou	13	H818-C139-3-2	K-feldspar/I	10.1	−77	5.1	314	This study
		H818-C139-2	K-feldspar/I	10.5	−103	5.3	314	
		H818-C139-3-1	Quartz/II	12.7	−103	4.9	277	
		H658-C121-3	Quartz/II	11.8	−92	4.0	277	
		H818-C121-3	Quartz/II	14.7	−92	6.9	277	
		13HB36	Quartz/II	13.7	−85	5.9		Wang (2016)
		13HB45	Quartz/II	13.1	−85	5.3		
		13HB50	Quartz/II	13.2	−80	5.4		
		13HB136	Quartz/II	13.1	−86	5.3		
		H1301	Quartz/II	13.5	−90	5.0	260	Hou (2011)
		H1303	Quartz/II	13.7	−78	5.2	260	
		H1310	Quartz/II	13.3	−85	4.8	260	
		HDM13-1	Quartz/II	13.1	−62	4.6	260	
		13HB139	Quartz/III	13.3	−82	4.0		Wang (2016)
	113	13HB06	Quartz/I	12.0	−88	6.5		Wang (2016)
		13HB15	Quartz/I	13.0	−74	7.5		
		H11343	Quartz/II	12.7	−81	4.2	260	Hou (2011)
		H11334	Quartz/II	13.1	−82	4.6	260	
		H11311	Quartz/II	12.4	−78	3.9	260	
		HSG4	Quartz/II	12.8	−68	4.3	260	
		13HB18	Quartz/II	12.6	−75	4.8		Wang (2016)
		WLS-9	Quartz/III	12.6	−83	4.1	260	Hou (2011)
		H11324	Quartz/III	12.3	−81	3.8	260	

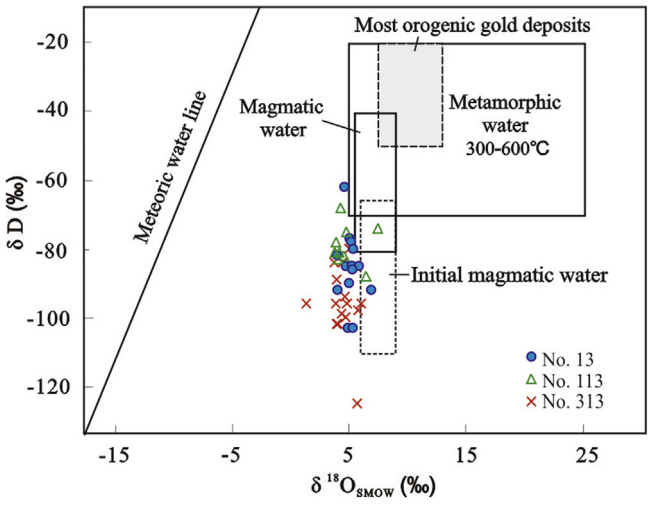

Fig. 8. Plot of δD vs. $\delta^{18}O$ for ore-forming fluids in the Hadamengou-Liubagou Au-Mo deposit. Fields for magmatic fluids after Taylor (1974), for initial magmatic water after Zhang (1985) and for most orogenic gold deposits after Goldfarb et al. (2004).

Eight samples gave Re-Os model ages from 374.1 ± 5.2 to 390.1 ± 5.4 Ma. The data yielded an isochron age of 383 ± 12 Ma and a weighted average age of 381.6 ± 4.3 Ma, with initial ^{187}Os of −0.07 ± 0.84, indicating that Mo mineralization occurred in Late Devonian.

5. Discussion

5.1. Source of ore-forming fluids, CO_2 and sulfur

The Hadamengou and the Liubagou ore blocks have similar H-O isotopic compositions. Most of the $\delta^{18}O_{H2O}$ and δD_{H2O} values of hydrothermal minerals vary from 3.5‰ to 5.5‰ and from −105‰ to −75‰, which are significantly different from those of metamorphic water ($\delta^{18}O$ 5‰–25‰, δD −70‰ to −20‰; Taylor, 1974) and the ore-forming fluids for most orogenic gold deposits (Goldfarb et al., 2004; Fig. 8). Most of the δD_{H2O} values fall within the range of magmatic fluids (−80‰ to −40‰; Taylor, 1974) and initial magmatic water (−110‰ to −65‰; Zhang, 1985) in equibrum with Au–Cu series granites, while the $\delta^{18}O_{H2O}$ values are consistent with or slightly lower than those of magmatic fluids (5.5‰ to 9.0‰, Taylor, 1974) and initial magmatic water (6.0‰ to 9.0‰, Zhang, 1985). It is thus suggested that the ore-forming fluids of the Hadamengou-Liubagou deposit were mainly derived from magmatic water with probably minor contribution of meteoric water, rather than metamorphic water.

In general, the source of carbon in ore-forming fluids may be derived from marine carbonate, organic matter, magmatic carbon, or some combination of the three (Hoefs, 2008). Given ore fluids with temperatures above 100 °C (Zhang, 2012) and the mineral assemblage of barite, pyrite and calcite indicating a relatively high fO_2 condition, then the $\delta^{13}C$ values of hydrothermal carbonates could represent the total carbon isotopic composition of ore-forming fluids, i.e., $\delta^{13}C_{carbonate} \approx \delta^{13}C_{\Sigma C}$ (Ohmoto, 1972). There is no systematic difference between Hadamengou and Liubagou in

Table 3
Carbon and oxygen isotopic compositions of hydrothermal minerals in the Hadamengou-Liubagou Au-Mo deposit.

Ore block	Vein No.	Sample No.	Mineral	$\delta^{13}C_{PDB}$ /‰	$\delta^{18}O_{PDB}$ /‰	$\delta^{18}O_{SMOW}$/‰	Data source
Liubagou	313	ZK11506-4	Calcite	−5.0	−17.1	13.3	This study
	313	ZK8304-16	Calcite	−5.5	−22.9	7.3	
	313	ZK10006-10	Calcite	−10.3	−15.1	15.3	
Hadamengou	13	LC-2	Ankerite	−5.1	−19.4	10.1	GHCAPF (1995)
	13	LC-3	Ankerite	−4.0	−26.5	3.7	
	13	LC-4	Calcite	−3.2	−17.8	11.8	
	13	HD378	Calcite	−3.2	−17.5	12.8	
	13	WK-HDMG-12	quartz	−3.9		12.9	Xie (2011)
	13	WK-HDMG-13	quartz	−3.4		12.4	
	113	Nhdm-7	quartz	−3.5		12.9	

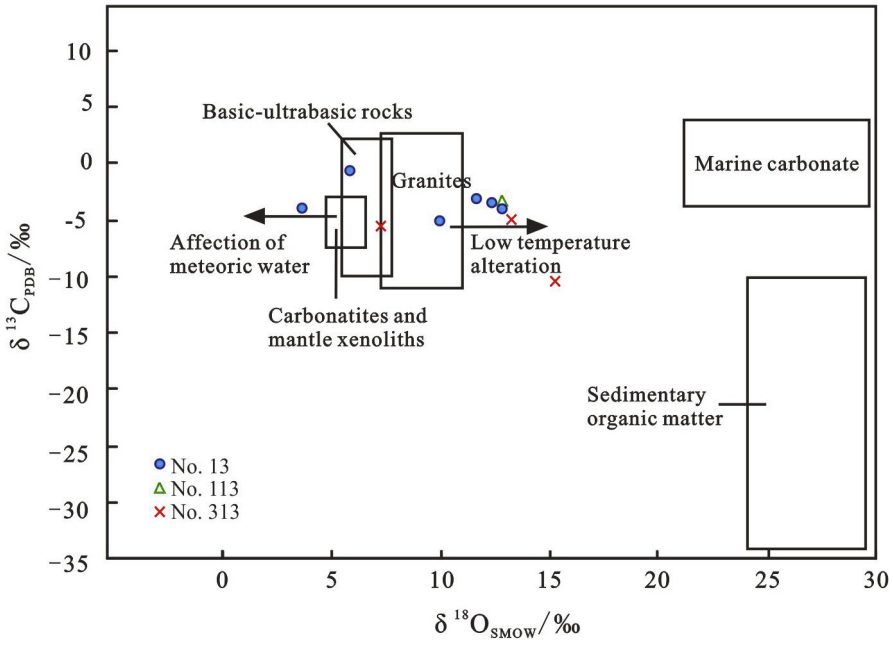

Fig. 9. $\delta^{13}C_{PDB}$ vs. $\delta^{18}O_{SMOW}$ diagram of hydrothermal carbonate minerals in the Hadamengou-Liubagou Au-Mo deposit.

terms of carbon isotopes. The $\delta^{13}C$ values of calcite and ankerite range from −5.5 ‰ to −3.2 ‰ with an average of −4.1 ‰ (except for one value at −10.3 ‰), suggesting a mantle (magmatic) carbon origin (−5‰; Hoefs, 2008). These values are relatively lower than those of marine carbonate (±0‰; Zhang, 1985) and significantly higher than sedimentary organic matter (−25 ± 5‰; Zhang, 1985), ruling out the possibility of contribution from these two carbon reservoirs. In the $\delta^{13}C$-$\delta^{18}O$ diagram, the wide variation of $\delta^{18}O$ values from 3.7‰ to 15.3‰ may reflect the increasing effect of low temperature alteration (Liu and Liu, 1997; Kontak and Kerrich, 1997).

Inasmuch as the sulfur isotopic composition of sulfur-bearing minerals is strongly controlled by the physico-chemical conditions (e.g., T, fo_2, pH) of hydrothermal fluids and the isotopic composition of sulfur ($\delta^{34}S_{\Sigma S}$) in the ore fluids, discussions on the source of sulfur must be based on the accurate determination of physico-chemical parameters and $\delta^{34}S_{\Sigma S}$ values (Ohmoto, 1972; Rye and Ohmoto, 1974). Sulfide minerals that precipitated in equilibrium with magnetite, hematite, or sulfate minerals could exhibit isotopic compositions markedly different from those of the depositing fluids. Therefore, the sulfur isotopic composition of minerals can be used to determine the $\delta^{34}S_{\Sigma S}$ value and the source of sulfur only when the temperature, fo_2 and pH conditions of ore-forming fluids are known (Ohmoto, 1972; Rye and Ohmoto, 1974). The wide variation on the $\delta^{34}S$ values of sulfides (−21.7‰ to 5.4‰, mostly −20‰ to 0‰) as well as the relatively uniform $\delta^{13}C$ values of carbonates (typically −5.5‰ to -3.2‰) from this deposit may suggest that the minerals were precipitated under relatively high fo_2 conditions (Ohmoto, 1972). Based on the mineral assemblage and microthermometric data from Liubagou, Zhang (2012) estimated the $lgfO_2$ to be in a range of −39 to −35. Fluid inclusion studies indicate that the temperatures of the ore fluids are around 270 °C at Liubagou and 280 °C–210 °C at Hadamengou, while the pH values are estimated to be 5.8–6.4 and 6.5–7.1, respectively (GHCAPF, 1995; Zhang, 2012). In a solution of T = 250 °C, I = 1, and $\delta^{34}S_{\Sigma S}$ = 0‰, as illustrated in Fig. 12, these physico-chemical parameters suggest that the $\delta^{34}S$ values of sulfides precipitated from the solution could vary between −26‰ and 1‰, which is consistent with the wide range of the sulfide $\delta^{34}S$ values of the deposit. Given that sulfate-bearing samples were collected from primary gold-bearing quartz veins, and the barite and celestite usually intergrown with the sulfides such as galena and chalcopyrite during main ore stage (Fig. 6E). The enrichment of ^{32}S in the sulfides during the main ore stage probably resulted in its depletion in the fluids and the relatively higher $\delta^{34}S$ values of sulfates (6.1‰–4.3‰). Therefore, the variable and typically negative $\delta^{34}S$ values of sulfides may indicate that the minerals were precipitated in the ore fluid of a magmatic origin with $\delta^{34}S_{\Sigma S} \approx 0$‰, rather than a biogenetic origin. In addition, the $\delta^{34}S$ values of pyrite from the Dahuabei granite are close to zero per mill (1.3‰–2.0‰, Nie and

Table 4
Sulfur isotopic compositions of sulfides and sulfates from the Hadamengou-Liubagou deposit and the Dahuabei granite.

Sample position	Ore vein/wall rock	Sample No.	Lithology	Mineral	$\delta^{34}S_{CDT}$/‰	Altitude/m	Data sources
Liubagou	313	ZK0402-12	Au-bearing altered rocks with sulfides	Pyrite	−6.8	1709	This study
		ZK16305-23	Au-bearing silicic-potassic altered rocks	Pyrite	−4.3	1146	
		ZK3603-8	Au-bearing silicic-potassic altered rocks	Pyrite	−8.4	1595	
		ZK3604-14	Au-bearing silicic-potassic altered rocks	Pyrite	−9.5	1477	
		PD2-8	Au-bearing silicic-potassic altered rocks	Pyrite	−11.9	1755	
		ZK3602-6	Au-bearing quartz veins	Pyrite	−9.1	1715	
		ZK16305-20-1	Au-bearing quartz veins	Pyrite	−11.2	1147	
		PD2-7	Au-bearing quartz veins	Pyrite	−12.7	1755	
		ZK2006-14	Au-bearing quartz veins	Pyrite	−14.1	1367	
		ZK2006-14	Au-bearing quartz veins	Galena	−15.4	1367	
		ZK9901-18	Au-bearing silicic-potassic altered rocks	Chalcopyrite	−11.9		
		LBG11	Au-bearing potassic altered rocks	Pyrite	−13.8		Hou (2011)
		LBG9	Au-bearing quartz veins	Pyrite	−12.5		
		LBG9	Au-bearing quartz veins	Galena	−15.1		
		LBG12	Au-bearing quartz veins	Galena	−14.7		
Hadaemgou	55	T55-1	Au-bearing silicic-potassic altered rocks	Pyrite	0.4		Guan et al. (1992)
	121	T121-1	Au-bearing silicic-potassic altered rocks	Pyrite	−4.8		
	12	T12-1	Au-bearing silicic-potassic altered rocks	Pyrite	−12.4		
		T12-2	Au-bearing silicic-potassic altered rocks	Pyrite	−11.7		
		T12-3	Au-bearing silicic-potassic altered rocks	Pyrite	−10.7		
	13	T13-1	Au-bearing silicic-potassic altered rocks	Pyrite	−11.3		
		T13-2	Au-bearing silicic-potassic altered rocks	Pyrite	−18.4		
		T13-3	Au-bearing silicic-potassic altered rocks	Pyrite	−13.0		
		T13-4	Au-bearing silicic-potassic altered rocks	Pyrite	−12.5		
		T13-5	Au-bearing silicic-potassic altered rocks	Pyrite	−14.0		
		H1307	Au-bearing potassic altered rocks	Pyrite	−0.2		Hou (2011)
		HDZK1	Au-bearing quartz veins	Pyrite	−17.0		
		H1302-1	Au-bearing potassic altered rocks	Pyrite	−12.5		
		H1303	Au-bearing quartz veins	Pyrite	−16.3		
		H1303	Au-bearing quartz veins	Galena	−21.7		
		WK-HDMG-12	Au-bearing quartz veins	Pyrite	−0.4		Xie (2011)
		WK-HDMG-12	Au-bearing quartz veins	Galena	−15.6		
	HE	W90-24	Au-bearing silicic-potassic altered rocks	Galena	−12.4		Nie and Bjorlykke (1994)
		W90-25	Au-bearing silicic-potassic altered rocks	Pyrite	−6.5		
		W90-26	Au-bearing silicic-potassic altered rocks	Pyrite	−8.5		
	26	W90-20	Au-bearing quartz veins	Pyrite	−2.5		
	113	W90-22	Au-bearing quartz veins	Pyrite	−8.4		
		W90-23	Au-bearing quartz veins	Pyrite	−7.0		
		T113-1	Au-bearing quartz veins	Pyrite	−11.7		Guan et al. (1992)
		T113-2	Au-bearing quartz veins	Pyrite	−7.0		
		T113-3	Au-bearing quartz veins	Galena	−15.1		
		T113-4	Au-bearing quartz veins	Galena	−15.4		
		T113-5	Au-bearing quartz veins	Galena	−10.3		
		T113-6	Au-bearing quartz veins	Chalcopyrite	−4.4		
		T113-7	Au-bearing quartz veins	Chalcopyrite	−9.3		
		T113-8	Au-bearing quartz veins	Chalcopyrite	−8.0		
		γs1-1	Au-bearing quartz veins	Galena	5.4		Lang and Li (1998)
		γs1-2	Au-bearing quartz veins	Pyrite	−14.8	1415	
		γs1-3	Au-bearing quartz veins	Chalcopyrite	−14.3		
		γs4-1	Au-bearing quartz veins	Chalcopyrite	−13.0		
		γs4-2	Au-bearing quartz veins	Galena	−14.9		
		h42	Au-bearing quartz veins	Pyrite	−3.9		
		h58-1	Au-bearing quartz veins	Galena	−14.7		
		h58-2	Au-bearing quartz veins	Pyrite	−14.1	1475	
		h84	Au-bearing quartz veins	Pyrite	−3.4		
		h187	Au-bearing quartz veins	Pyrite	−15.3	1240	
		h194	Au-bearing quartz veins	Pyrite	−1.2	1065	
		h228	Au-bearing quartz veins	Pyrite	−4.8		
		h231	Au-bearing quartz veins	Pyrite	−5.2		
		h233	Au-bearing quartz veins	Pyrite	−9.9		
		h236	Au-bearing quartz veins	Pyrite	−9.6		
		h6	Au-bearing quartz veins	Galena	−15.3		
		h6-1	Au-bearing quartz veins	Pyrite	−16.2		
		dn	Au-bearing quartz veins	Galena	−18.4		
		WLS-10	Au-bearing silicic-potassic altered rocks	Pyrite	−12.3	1305	Hou (2011)
		H11311	Au-bearing quartz veins	Pyrite	−11.3	1305	
		H11324	Au-bearing quartz veins	Pyrite	−5.9	1265	
		HSG2	Au-bearing quartz veins	Pyrite	−0.3	Surface	
		H11341	Au-bearing potassic altered rocks	Pyrite	−10.4	1185	
		H11342	Au-bearing quartz veins	Pyrite	−13.4	1185	
		H11342	Au-bearing quartz veins	Galena	−19.4	1185	

Table 4 (*continued*)

Sample position	Ore vein/wall rock	Sample No.	Lithology	Mineral	$\delta^{34}S_{CDT}$/‰	Altitude/m	Data sources
		HSG4	Au-bearing quartz veins	Pyrite	−12.2	Surface	
		HSG4	Au-bearing quartz veins	Galena	3.1	Surface	
		WLS-9	Au-bearing quartz veins	Galena	−13.7	1305	
		Nhdm-7	Au-bearing quartz veins	Pyrite	2.0		Xie (2011)
		Nhdm-10	Au-bearing quartz veins	Pyrite	−13.8		
	78	W-78	Au-bearing quartz veins	Galena	−15.1		Lang and Li (1998)
		78-63	Au-bearing quartz veins	Galena	−17.3		
		W1s02	Au-bearing quartz veins	Pyrite	−1.9		
		W1s010	Au-bearing quartz veins	Pyrite	−2.4		
		W90-27	Au-bearing quartz veins	Galena	−13.5		Nie and Bjorlykke (1994)
		W90-28	Au-bearing quartz veins	Pyrite	−8.2		
		W90-29	Au-bearing quartz veins	Pyrite	−7.9		
	HW	W90-21	Au-bearing silicic-potassic altered rocks	Pyrite	−3.8		
		W90-30	Au-bearing silicic-potassic altered rocks	Galena	−12.3		
		W90-31	Au-bearing silicic-potassic altered rocks	Pyrite	−7.5		
		W90-32	Au-bearing silicic-potassic altered rocks	Pyrite	−8.4		
		16-187-1	Au-bearing quartz veins	Barite	6.1		GHCAPF (1995)
		5-109	Au-bearing quartz veins	Celestite	4.3		
Dahuabei		W90-55	Granite	Pyrite	1.3		Nie and Bjorlykke (1994)
		W90-57	Granite	Pyrite	2.0		

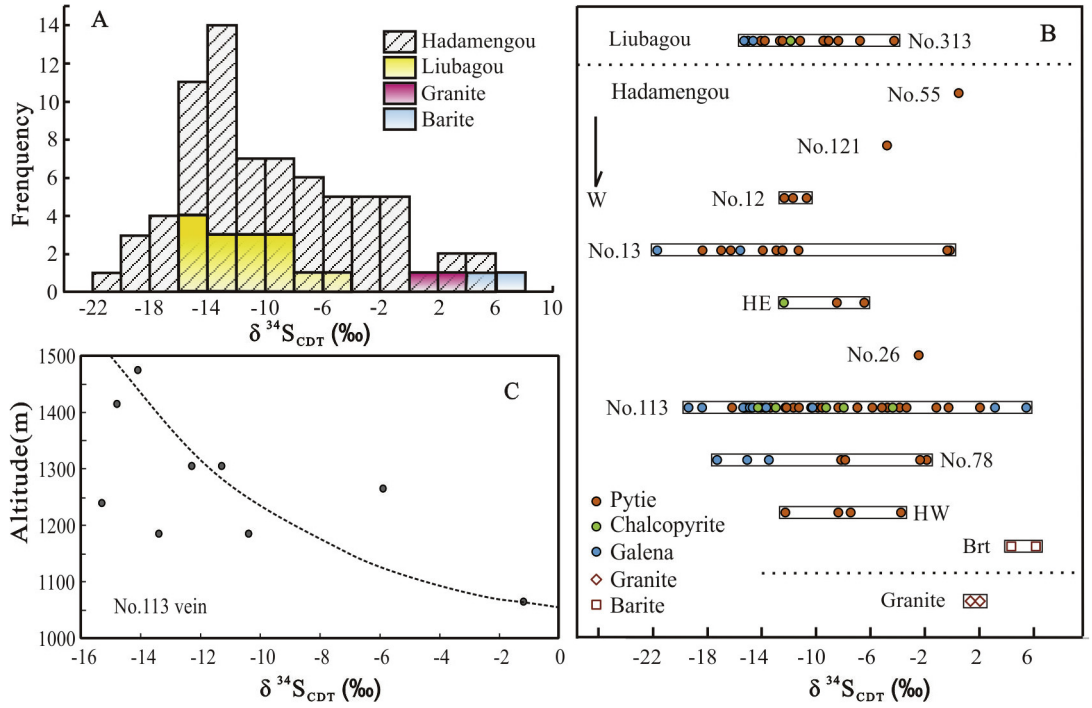

Fig. 10. Frequency histogram of $\delta^{34}S$ in sulfides and sulfates (A), sulfur isotopic comparison for different minerals and ore veins (B), and correlation between the $\delta^{34}S$ values of sulfides and the elevations of samples from ore vein No.113 (C) at Hadamengou-Liubagou.

Bjorlykke, 1994), suggesting a magmatic source of sulfur and implying a possible link between the mineralization at Hadamengou-Liubagou and the magmatic activity.

The sulfides from Liubagou have a markedly narrower range of $\delta^{34}S$ values (−15.4‰ to −4.3‰, mostly −15‰ to −9‰) than those from Hadamengou (−21.7‰ to 5.4‰, mostly −20‰ to 0‰), suggesting that the former was precipitated under a narrower $lgfO_2$ range of −36 to −37 than the latter (−36.5 to −38.5). It is also noted that a roughly negative correlation exists between the $\delta^{34}S$ values of sulfides and the elevations of samples from ore vein No.113 at Hadamengou (Fig. 10C). Based on the field observation of similar mineral assemblage and metal element distribution, the differential erosion is not apparent in the single ore vein No. 113. A possible explanation is that the isotopically lighter sulfur (^{32}S) may tend to be enriched in the fluids ascended to a higher level due to dynamic fractionation. Alternatively, the ore fluids at the shallower parts of the deposit may be more oxidized and the preferential fractionation of ^{34}S in oxidized species of sulfur in the fluids could result in the lower $\delta^{34}S$ values of sulfides.

5.2. Timing of Au-Mo mineralization and magma emplacement

The timing of mineralization and, in particular, the temporal relationship between the gold and molybdenum mineralization in the Hadamengou-Liubagou deposit are still in dispute because of the lack of detailed paragenetic studies and suitable minerals

Table 5
Re-Os isotopic data and model ages of molybdenite from the ore vein No. 113 at Hadamengou Au-Mo deposit.

Sample	Weight/g	w(Re)/10^{-6}		w(Os)/10^{-9}		w(^{187}Re)/10^{-6}		w(^{187}Os)/10^{-9}		Model age/Ma	
		Value	Uncertainty	Value	Uncertainty	Value	Uncertainty	Value	Uncertainty	Value	Uncertainty
113-1	0.05067	5.968	0.048	0.0034	0.0153	3.751	0.030	23.70	0.19	378.0	5.3
113-2	0.05006	9.291	0.072	0.0047	0.0052	5.839	0.045	37.75	0.30	386.8	5.3
113-3	0.05055	2.182	0.018	0.0058	0.0183	1.371	0.011	8.70	0.07	379.4	5.4
113-4	0.05170	1.798	0.014	0.0426	0.0048	1.130	0.009	7.12	0.07	376.9	5.6
113-5	0.05042	8.473	0.064	0.0482	0.0195	5.325	0.041	33.30	0.28	374.1	5.2
113-6	0.05066	4.070	0.033	0.2700	0.0282	2.558	0.021	16.53	0.15	386.6	5.6
113-7	0.04029	7.801	0.059	0.0446	0.0170	4.903	0.037	31.97	0.27	390.1	5.4
113-8	0.01628	10.210	0.080	0.0136	0.0305	6.420	0.050	40.94	0.34	381.5	5.3

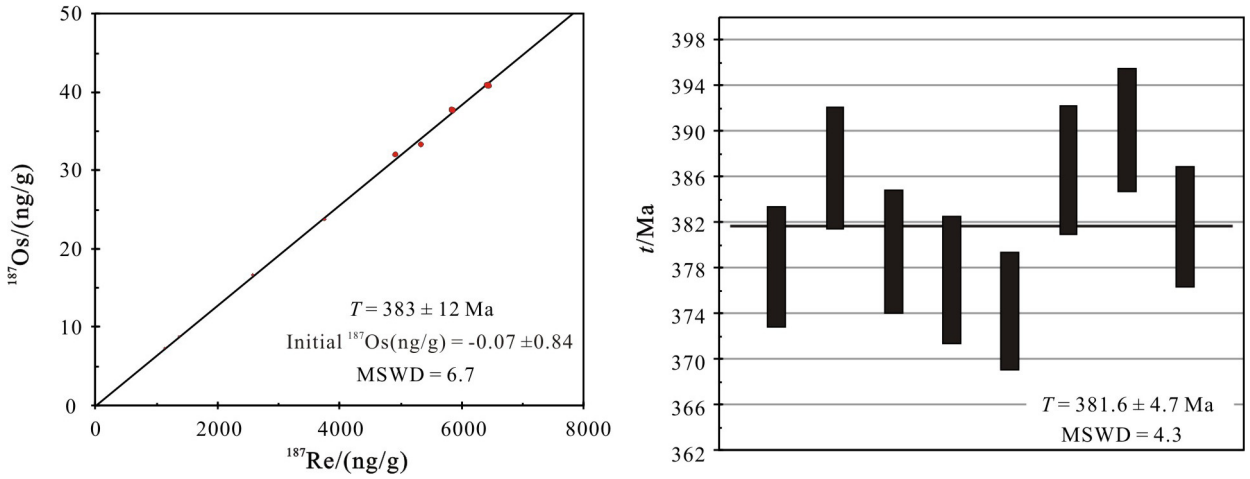

Fig. 11. Re-Os isochron age (A) and weighted average age (B) of molybdenite from the Hadamengou-Liubagou Au-Mo deposit.

for isotopic dating. The Re-Os isotopic dating on molybdenite of this study indicates that the Mo mineralization at Hadamengou occurred in Late Devonian at ~382 Ma. However, a few previous studies based on different geochronologic methods outlined a wide range of ages from the Early Carboniferous to Late Triassic (355–203 Ma). In the Hadamengou ore block, for example, K-Ar isotopic dating on the sericite in altered rocks yielded an age range of 276–248 Ma (Lang, 1990; GHCAPF, 1995; Zhang et al., 1999; Meng et al., 2002), while Rb-Sr isotopic dating on the altered whole rocks defined an age of 287–203 Ma (Nie, 1995). Hart et al. (2002) analyzed the fuchsite at Hadamengou and obtained the oldest step ^{40}Ar-^{39}Ar age of 351.8 ± 0.8 Ma that is interpreted to be the minimum age of mineralization and temporally related to the Dahuabei Batholith. Recent stepwise ^{40}Ar-^{39}Ar dates on sericite separated from ore vein No. 13 at Hadamengou obtained a plateau date of 239.8 ± 3.0 Ma, while the ^{40}Ar-^{39}Ar isochron age of the sericite from altered rocks is 322.6 ± 3.2 Ma (Nie et al., 2005). In the Liubagou ore block, ^{40}Ar-^{39}Ar isotopic dating on K-feldspar from altered ores gave a plateau age of 217.9 ± 3.1 Ma (Zhang et al., 2011b), while recent Re-Os dating on one molybdenite sample yielded a model age of 354.9 ± 5.7 Ma (Wang et al., 2014).

The wide range of the reported ages using different isotopic dating methods has made it difficult to ascertain if a given isotopic date relates to the gold and/or molybdenum mineralization. Among the different methods noted above, the K-Ar and Rb-Sr dates are probably most questionable, because K- and Rb-bearing minerals (e.g., K-feldspar, biotite, muscovite, and sericite) are sensitive to postdepositional heating and/or alteration and may have been isotopically reset (Faure and Mensing, 2005). Consequently, the stepwise ^{40}Ar-^{39}Ar ages mentioned above and the Re-Os dates of molybdenite obtained in this study may provide the most reliable age constraints on the mineralization for the Hadamengou-Liubagou deposit. These ages roughly outline two ranges of mineralizing events of 382–323 Ma and 240–218 Ma that correspond to the Late Devonian to Early Carboniferous (Variscan) and the Middle to Late Triassic (Indosinian), respectively.

There exists linkage between Au-Mo mineralization and protracted magmatic event. One Re-Os model age of molybdenite at Liubagou (355 Ma, Wang et al., 2014) and ^{40}Ar-^{39}Ar ages at Hadamengou (352–323 Ma, Hart et al., 2002; Nie et al., 2005) overlap with the intrusion age of the Dahuabei Batholith (366–330 Ma, Miao et al., 2000; Li et al., 2009; Zhang, 2012), implying that the mineralization was related to magmatic hydrothermal fluids of the same period when the Dahuabei Batholith intruded. The Re-Os age of 381.6 ± 4.3 Ma at Hadamengou in this study is earlier than the oldest age of the Dahuabei Batholith (365.5 ± 7.3 Ma, Zhang, 2012) obtained so far. Based on the errors of Re-Os and U-Pb dating, the age difference between Mo mineralization and magmatism is 5–27 Ma. Considering that the Dahuabei Batholith is a complex formed during large age span (>30 Ma), an earlier intrusion age coinciding to Re-Os dating is quite possible. Thus, the Variscan mineralization event is approximately consistent with the intrusive age of the Dahuabei Batholith (366–330 Ma) and the molybdenium mineralization at Hadamengou and Liubagou (382–355 Ma). By the same token, the Indosinian mineralization event roughly corresponds to the magmatic activity at Xishadegai and Shadegai (~233 Ma), as well as the Mo mineralization at Xishadegai (~225 Ma, Zhang et al., 2011a).

Therefore, there exist at least two major episodes of Mo mineralization at Hadamengou-Liubagou and its adjacent region, namely around 382–355 Ma and ~225 Ma. However, it is still unclear whether the Au mineralization in the study area was related to one or both of these two episodes. Some previous researchers thought that the gold mineralization was almost coeval with or a

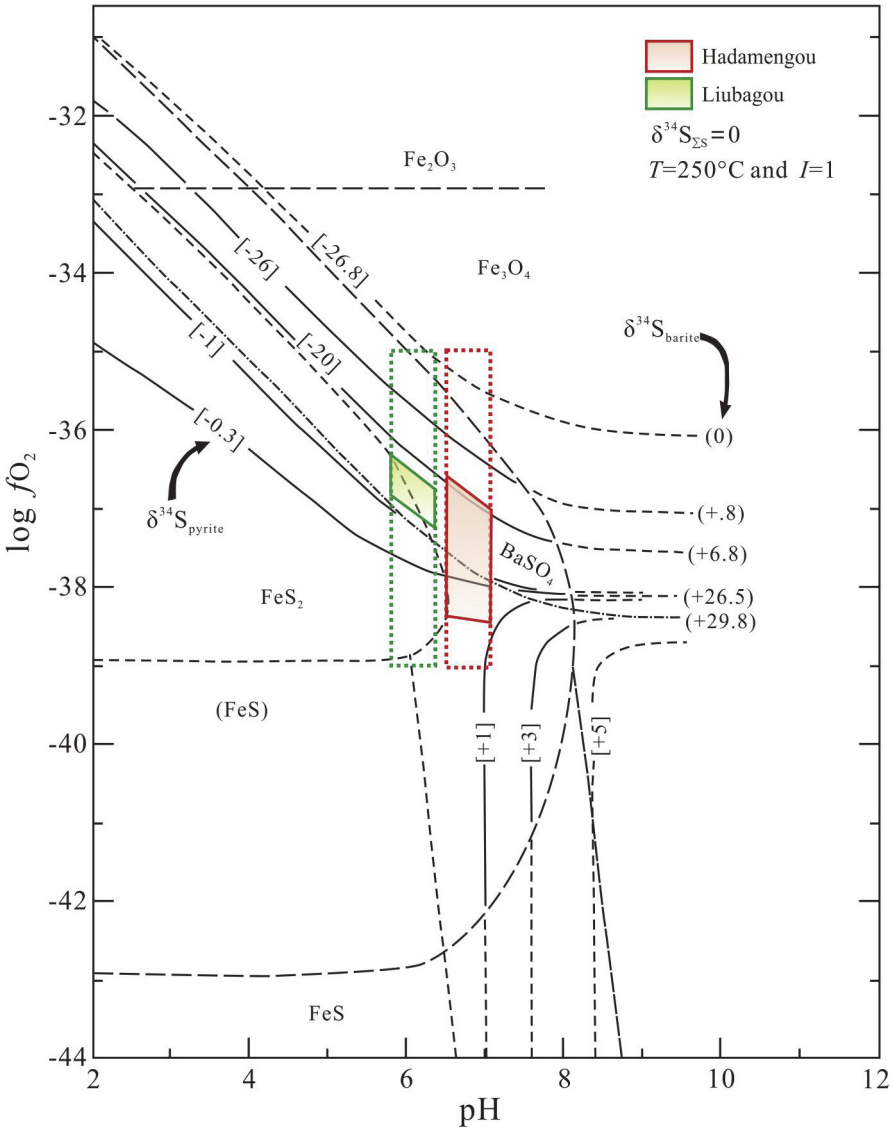

Fig. 12. Plot of sulfur isotopic compositions of sulfur-bearing minerals in the $\delta^{34}S_{\Sigma S}=0$ system for the Hadamengou-Liubagou Au-Mo deposit (after Ohmoto, 1972). ——, ·····, -·-·-: $\delta^{34}S$ contours. Values in [ ] and ( ) are, respectively, for pyrite and barite at $\delta^{34}S_{\Sigma S}=0‰$. – – – –: Fe-S-O mineral boundaries at $\Sigma S=0.1$ moles/kg H_2O. - - - - -: Fe-S-O mineral boundaries at $\Sigma S=0.001$ moles/kg H_2O. -·-·-·-: barite soluble/insoluble boundary at $m^{2+}_{Ba}\cdot m_{\Sigma S}=10^{-4}$.

little earlier than the precipitation of molybdenite (Hou et al., 2011). In contrast, our petrographic studies on textures, crosscutting relationships, and mineral assemblages of the ores indicate that gold was precipitated markedly later than the Mo mineralization. Molybdenite is typically observed only in the earliest stage (I) mineral assemblage, either as deformed and sinuous veinlets in association with K-feldspar, biotite, pyrite and carbonate minerals in the potassic altered rocks, or less commonly as deformed thin platy crystals pervasively distributed in the altered rocks. The molybdenite-bearing veinlets are usually fractured and cemented or crosscut by minerals of later stages (II, III and IV), including quartz, pyrite, barite, calcite, and ankerite. Gold occurs predominantly in the stage III mineral assemblage, either infilling microfissures or included in pyrite and quartz or, less commonly, occurring at the margin of dolomite (Figs. 6A-C), although it is occasionally also observed as very fine grains in the K-feldspar and quartz of stages I and II. Thus, a distinct tectonic deformation must have happened and separated the molybdenium and gold mineralization. From a broad perspective, the final closure of the Paleo-Asian Ocean and the suturing between the Siberian and NCC occurred in Late Permian and the post-collisional extension in Triassic resulted in the revival of EW-trending fault zones and the intrusion of widespread alkaline granites along the northern margin of NCC (Yan et al., 2000; Wu et al., 2002; Xiao et al., 2003; Li, 2006; Windley et al., 2007). Given that the tectonic deformation responsible for the fracturing of the Mo ores was related to this syn- to post-collisional orogeny, the peak Au mineralization in the study area may most probably have occurred during the Indosinian, roughly corresponding to the magmatic activity at Xishadegai and Shadegai and the Mo mineralization at Xishadegai.

5.3. Implication for ore genesis

Regarding the genesis of ore precipitation and its relationship to metamorphism, magmatism and tectonic deformation, the deposit has been the subject of continued debate. Gan et al. (1994) suggested that gold was mainly sourced from metamorphic rocks during the Neoproterozoic tectono-thermal event. GHCAPF (1995) proposed that the deposit is genetically related to the Caledonian to Variscan pegmatite. Nie (1995) believed that the gold deposit

mainly formed during the Variscan tectonic movement and is genetically related to the Dahuabei Batholith. Nie et al. (2005) rediscussed gold mineralization time at Hadamengou based on ^{40}Ar-^{39}Ar isotopic studies and proposed that the deposit was mainly formed during the Early Indosinian tectonic movement.

Several lines of geologic, petrographic and isotopic evidence presented in this study suggest that the molybdenum and gold mineralization is of magmatic hydrothermal origin, rather than a metamorphic origin. Alkaline granites of the Variscan and Indosinian epochs are regionally well developed with three representative intrusions at Dahuabei, Xishadegai and Shadegai situated approximately 5–15 km to the west and north of the Hadamengou-Liubagou Au-Mo deposit. The rough agreement in the timing of the mineralization and the magma emplacement in the study area, as noted above, implies the magmatic hydrothermal nature of the deposit. As one of the most striking features of the deposit, the widespread potassic alteration that is a common characteristic of many magmatic-related ore deposits (Saunders and Tuach, 1991; Müller and Groves, 1997; Sillitoe and Thompson, 1998; Chen and Li, 2009; Sillitoe, 2010; Éric et al., 2015) highlights a dominant magmatic source of the hydrothermal fluids. The presence of Te-bearing minerals such as calaverite and altaite in the main ore stage mineral assemblage is also an indication of magmatic affinity (Lang and Baker, 2001; Cooke and McPhail, 2001; Tombros et al., 2010; Éric et al., 2015). Isotopic data provide further constraints on the ore genesis. Hydrogen and oxygen isotopes indicate a major contribution of magmatic water, while C and S isotopes suggest that the carbon and sulfur in the ore fluids were also mainly derived from magma. In addition, fluid inclusion studies indicate that the mineralization was related to the NaCl-H_2O-CO_2 fluid system with typical homogenization temperatures of 200 °C–350°C and salinities of 5%–43 wt% NaCl eq. (Shen et al., 2010; Zhang, 2012). Hypersaline, halite- and opaque mineral-bearing inclusions are commonly observed in the main ore stage mineral assemblages. Such a fluid is typical for many intrusion-related hydrothermal ore deposits (Baker, 2002; Chen et al., 2007, 2009; Chen and Li, 2009; Klemm et al., 2008; Éric et al., 2015; Melfos and Voudouris, 2016; Wang et al., 2016a), but remarkably different from the metamorphic fluids in typical orogenic gold deposits (e.g., Groves et al., 1998; Ridley and Diamond, 2000; Goldfarb et al., 2004; Chen et al., 2007; Fairmaid et al., 2011). Above geological and isotopic evidence led us to conclude that the Hadamengou-Liubagou deposit is related to alkaline intrusions, and can be regarded as a magmatic hydrothermal vein type gold deposit, rather than orogenic gold deposit.

Based on the foregoing discussion, a possible genetic model for the Au-Mo mineralization of the Hadamengou-Liubagou deposit is illustrated in Fig. 13. During Devonian to Early Carboniferous, southward subduction of the Paleo-Asian Ocean beneath the NCC (Xiao et al., 2003; Zhang and Zhai, 2010) triggered the revival of the Baotou-Hohhot Fault and the emplacement of the Dahuabei alkaline granitic Batholith in the study area. The magma-derived hydrothermal fluids transported Mo and possibly minor Au along the branch faults and interacted with gneiss, forming potassic-silicifed envelopes with Mo mineralization. This subduction continued until the Early Permian. The Paleo-Asian Ocean closed and the Siberian and NCC was finally collided in the Late Permian along the Solonker suture zone (Xiao et al., 2003; Li, 2006; Windley et al., 2007). Later in the Triassic, the post-collisional extension resulted in the revival of EW-trending fault zones and the emplacement of the alkaline granites at Xishadegai and Shadegai. The magmatic hydrothermal fluids transported both Au and Mo and were responsible for the major gold mineralization at Hadamengou-Liubagou and the porphyry molybdenum mineralization at Xishadegai. Regionally, about 19 Mo deposits and 5 Au deposits are believed to be spatially and temporally related to this magmatic event (Nie et al., 2011).

5.4. Comparison to adjacent areas

Mineral deposits are generally sensitive indicators of geodynamic environments and their time-space distribution is used to assess the tectonic evolution (Groves et al., 2005; Groves and Bierlein, 2007; Dill, 2010). Major magmatic hydrothermal Cu, Au, and Mo deposits of CAMD are distributed from the Urals Mountains in Russia in the west, through Mongolia to north-eastern China (Seltmann et al., 2014; Zeng et al., 2015; Xue et al., 2016). These deposits are intimately related to multiple magmatic episodes during the evolution of the Altaid and Transbaikal-Mongolian orogenic collages from the Ordovician to the Jurassic (Groves et al., 2005; Seltmann and Porter, 2005; Seltmann et al., 2014; Zeng et al., 2015). The Hadamengou-Liubagou area, located in the mideast of the CAMD, displays two mineralizing events associated with magmatic activities, namely the Variscan Mo mineralization (382–355 Ma) and Indosinian Au, Mo mineralization (240–218 Ma). For comparison, representative magmatic hydrothermal deposits of similar mineralization age are summarized in Table 6. The emplacement location of these deposits is shown on Fig. 1 and Fig. 14. The collective data set provides a comprehensive temporal framework for magmatic hydrothermal mineralization in CAMD (Table 6). With the exception of the Ordovician porphyry Cu–Au/Mo deposits such as Bozshakol, Andash, Taldy Bulak, Duo-Baoshan and Tongshan (Seltmann and Porter, 2005; Seltmann et al., 2014), all the Cu, Au, and Mo deposits in CAMD formed from Devonian to Triassic. Geochronological dating has documented two episodes of mineralization: Late Devonian to Early Carboniferous (382–323 Ma) and Late Permian to Triassic (260–220 Ma).

5.4.1. Late Devonian to Early Carboniferous mineralization and tectonic setting

The Late Devonian to Early Carboniferous magmatic hydrothermal deposits are mainly distributed in the west and mideast of CAMD, and are formed in an island-arc setting (Table 6 and references cited therein). From west to east, the Late Paleozoic deposits in CAMD occur in different magmatic arcs, such as Urals-Zharma, Valerianov-Beltau-Kurama, Kipchak and Kazakh-Mongol (Fig. 14, Seltmann et al., 2014). The Hadamengou-Liubagou deposit is located in the south margin of Kazakh-Mongol magmatic arc (Fig. 14) which hosts Kounrad, Aktogai and Koksai of Kazakhstan, Oyu Tolgoi and Tsagaan Suvarga of Mongolia, as well as Tuwu-Yandong of Xinjiang. Comparison of these deposits along Kazakh-Mongol magmatic arc provides useful information on geodynamic setting of ore formation.

In respect of ore type, most Cu-Au and Cu-Mo deposits in CAMD are porphyry type (Seltmann and Porter, 2005; Seltmann et al., 2014; Wang et al., 2015a,b; 2016a,b; Xue et al., 2016), while the Hadamengou-Liubagou deposit is hydrothermal vein type associated with potassic alteration dominated by K-feldspar. On the ages of ore formation, the Kounrad, Aktogai, Koksai and Tuwu-Yandong, located in the west of the Kazakh-Mongol magmatic arc, are formed in Early Carboniferous (323–331 Ma, Seltmann, 2004; Chen et al., 2014; Shen et al., 2015; Li, G.M. et al., 2016; Cao et al., 2016); while the Oyu Tolgoi, Tsagaan Suvarga and Hadamengou-Liubagou, located in the mideast, are formed in Late Devonian (370–382 Ma, Watanabe and Stein, 2000; Kirwin et al., 2005; Wainwright et al., 2011; Zeng et al., 2015). During the Late Devonian to Early Carboniferous, Kazakh-Mongol belongs to Andean-type magmatic arc resulting from the subduction of oceanic crust (Abdulin et al., 1998; Chen et al., 2014; Seltmann et al., 2014; Shen et al., 2015; Cao et al., 2016; Li, G.M. et al., 2016). The Cu-Au mineralization in mideast is ~50 Ma older than the west of Kazakh-Mongol magmatic arc, indicating the maturity of island arc evolves from Late Devonian to Early Carboniferous (Xue et al., 2016). On deposit scale, there are many large to giant

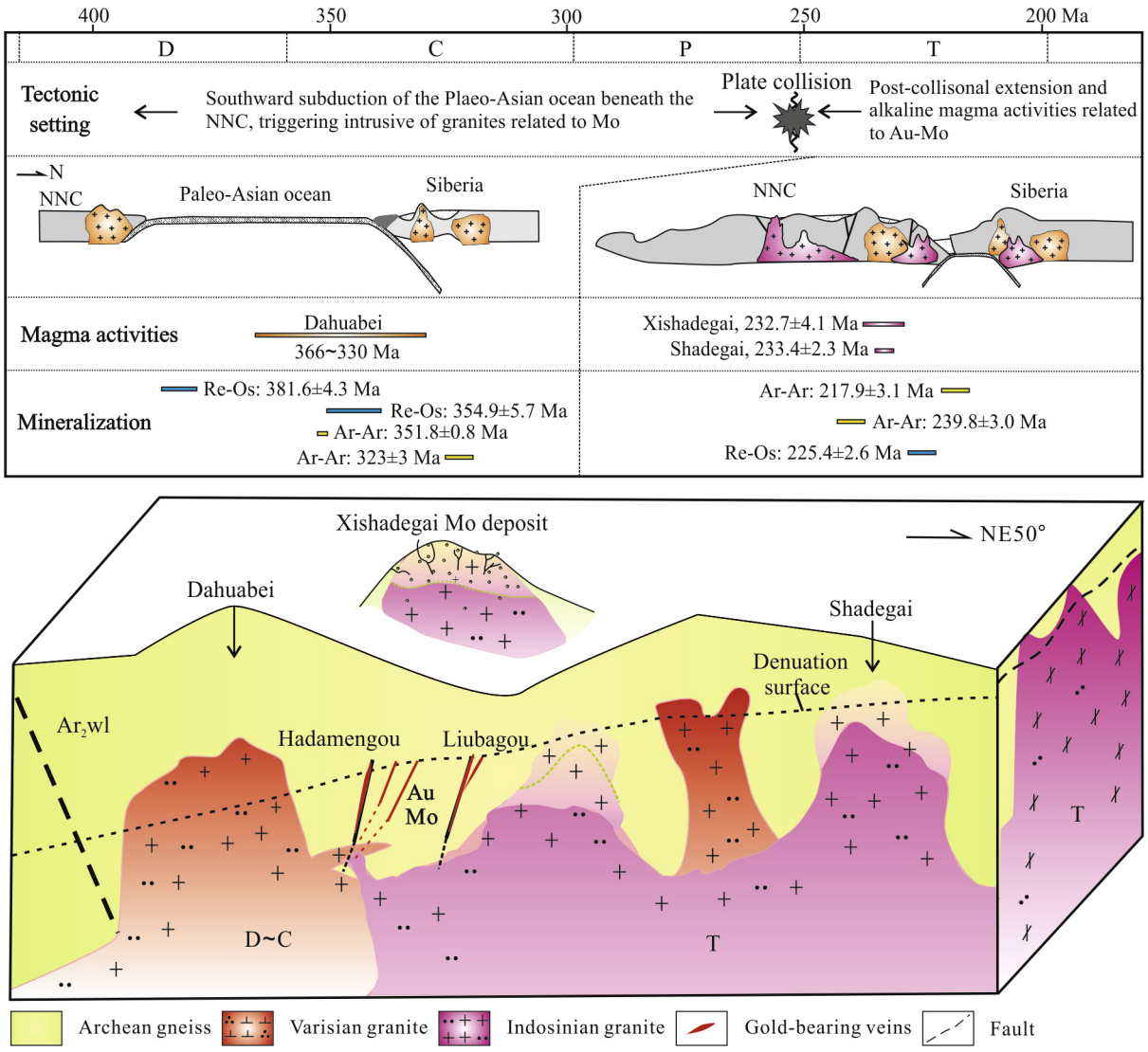

Fig. 13. Schematic presentation of a possible genetic model for gold and molybdenum mineralization in the Hadamengou-Liubagou area. Abbreviations: D–C = Devonian to Carboniferous, P = Permian, T = Triassic, NNC = North China Craton.

deposits in the Kazakh-Mongol magmatic arc, however, the Mo reserves at Hadamengou-Liubagou are small in scale. As for metal association, Cu-Au and Cu-Mo are predominant in this belt, however, only Mo mineralization developed at Hadamengou-Liubagou in Devonian. Because porphyry Cu and Mo systems typically span the upper ~4 km and ~6 km of the crust (Sillitoe, 2010), the Tsagaan Suvarga Cu-Mo deposit and Hadamengou-Liubagou Mo occurrence might undergo a certain extent of denudation. Despite of the above differences, the spatially adjacent of Oyu Tolgoi, Tsagaan Suvarga and Hadamengou-Liubagou, the contemporaneous mineralization ages, and the intimate relationship with magma activity suggest that they are products under the same subduction tectonic setting.

5.4.2. Late Permian to Triassic mineralization and tectonic setting

The Late Permian to Triassic magmatic hydrothermal deposits are mainly distributed in the mideast of CAMD, especially in Mongolia and Inner Mongolia along the north margin of NNC (Fig. 1, Fig. 14). Previous studies on stratigraphy, palaeontology, paleogeography, lithofacies, magmatic, and metamorphic events indicate that the suture lies in the Suolunshan-Xar Moron river-Changchun-Yanji belt, and the final closing of the Paleo-Asian Ocean took place from Late Permian to Early Triassic (Li, 1998; Li et al., 2006; Shi, 2006; Wang and Fan, 1997; Wang et al., 2008; Wang and Guo, 2012; Cao et al., 2013; Zeng et al., 2012, 2015). Thus, porphyry and hydrothermal vein-type deposits in CAMD were formed in a syn-collisional to post-collisional tectonic setting (Table 6 and references cited therein).

The metal association includes Mo-Cu, Mo and Au. The Mo-Cu deposits such as Chaganhua, Chagandeersi, Laojiagou, Baituyingzi, Kulitu and Baimashi outline an age range from 243 to 249 Ma (Cai et al., 2011a,b; Zeng et al., 2012; Sun et al., 2013); while the Mo deposits including Baishan, Xiaohulishan and Xishadegai formed from 225 to 229 Ma (Li et al., 2006; Peng et al., 2010; Zhang et al., 2011a; Wang et al., 2016c). The increase of Mo/Cu ratios may reflect tectonic evolution to a certain extent (Sun et al., 2013). The Mo-Cu deposits of Late Permian to Early Triassic were formed in a syn-collisional tectonic setting (Zeng et al., 2012, 2015; Sun et al., 2013). The partial melting of magma contributes high copper contents during Mo-Cu mineralization (Chen et al., 2009; Sun et al., 2013). The Middle to Late Triassic porphyry Mo deposits are formed in a post-collisional to intracontinental extensional environment (Zhang et al., 2011a; Yang et al., 2013; Zhu et al., 2013; Wang et al., 2015). The magmatism dominated by fractional crystallization might result in Mo deposits without other accompanying metal resources (Zhang et al., 2010; Sun et al.,

Table 6
Characteristics of the Cu, Au, Mo deposits in the Central Asia Metallogenic Domain.

Deposit	Location	Deposit type	Commodity	Geodynamic setting	Major host rocks	Ore forming ages (Ma)	Ore textures	Major metal minerals	Alteration assemblage	References
Taldy Bulak Levoberezhny	Kyrgyzstan	Porphyry-Mesothermal	Au, Cu	Kipchak and Kazakh-Mongol magmatic arcs	Diorite porphyry	Devonian	Vein, stockwork	Py, Cp, Gn, Ars, Sph, Gl	Q, Ser, Cb, Tur	Seltmann (2004) and Seltmann et al. (2014)
Yubileinoe	Kazakhstan	Porphyry	Au, Cu	Urals-Zharma magmatic arc	Plagiogranite porphyry, granodiorite, and volcanic wallrocks	~380 Ma	Stockwork, disseminated	Py, Mt, Cp, Ars, Td, Snt, Gl, with minor Sph, Gn, Sh, Mot, Bo	Potassic and phyllic alteration	Seltmann (2004) and Seltmann et al. (2014)
Oyu Tolgoi	Mongolia		Cu, Au	Kazakh–Mongol magmatic arc	Porphyritic quartz monzodiorite, granodiorite	373 Ma*	Disseminated, stockwork, and breccia	Bo, Cha, Py, Enr, Ten, Mot	Potassic (Bi-Mt-Kf) , Q–Ser, argillic; and propylitic alteration	Perello et al. (2001), Kirwin et al. (2005), Wainwright et al. (2011)
Tsagaan Suvarga	Mongolia		Cu, Mo		Monzogranite porphyry	370 Ma*	Disseminated, stockwork	Cp, Bo, Mot, Py	Potassic alteration, sericitization, argilligation, and prophyllic alteration.	Watanabe and Stein (2000), Seltmann et al. (2014), Zeng et al. (2015)
Tuwu-Yandong	China, (Xinjiang)		Cu, Au	Dananhu-Tousuquan island arc: active continental margin of the Tarim Plate	Granodiorite-, plagiogranite-porphyries	323 Ma*	Veinlet-disseminated, veinlet-like and less commonly nodular	Cp, Py with less Bo, Cha, Dg, Sph	Potassic (Bi-Q), intermediate argillic (Ill-Ch ± Ab), and phyllic (Ill-Py-Q))	Rui and Zhang (2002), Shen et al. (2014a,b), (2015), Han et al. (2006), Wang et al.,(2015a, b)
Koksai	Kazakhstan		Cu, Au	Kazakh–Mongol magmatic arc: Andean-type magmatic arc in the Devonian to the Late Carboniferous, resulting from the subduction of Junggar-Balkhash oceanic crust	Granodiorite porphyry	Carboniferous	Veinlet-disseminated	Py, Cp, Mt, Bo, Mot	Potassic (Q-Kf), intermediate argillic (Q-Ill-Ch), propylitic (Cal)	Mutschler et al. (2000), Seltmann (2004), Shen et al. (2015)
Kounrad	Kazakhstan		Cu, Au		Granitoid rocks	325–327 Ma	Vein stockworks andbreccias	Py, Cp, Bo, Mot, Enr, Td, Cha, with less Sph, Gn, Ars, Ten	Potassic (Bi-Kf), phyllic (Q-Ill), propylitic (Py-Q-Ill-Ch-Cb), argillic (Q-Kln)	Kudryavtsev (1996), Chen et al. (2014), Li, G.M. et al. (2016)
Aktogai	Kazakhstan		Cu, Au		Granodiorite, tonalite porphyry	327–331 Ma	Chalcopyrite-quartz veinlets	Py, Cp, Bo, Cha, Mot, Sph, Gn, Gl	Potassic (Q-Bi-Kf), phyllic (Q-Ill), propylitic (Q-Ill-Ch-Cb)	Abdulin et al. (1998), Chen et al. (2014), Cao et al. (2016)
Benqala	Kazakhstan		Au, Cu	Valerianov-Beltau-Kuramamagmatic arc	Porphyritic quartz diorite, granodiorite and plagiogranite porphyries	Carboniferous	Stockwork	Py, Cp, Mt, with minor Mot, Bo, Cha	Potassic (Ab-Kf-Bi), propylitic (Ch-Ep-Prh), overprinted by a Q–Ser assemblage	Seltmann (2004)
Erdenet	Mongolia		Cu, Mo	Selanga-Gobi-Khanka magmatic arc, along the active continental margin of the Siberian Craton	Diorite, diorite porphyry, and granodiorite	241 Ma*	Disseminated, stockwork, and breccia	Cp, Bo, Cha, Py, Mot, Pyr, Ten, with less Sph, Gn, Mt	Potassic (Q-Kf), medial phyllic (Q-Ill), argillic (Ill)	Watanabe and Stein (2000), Jiang et al. (2010), Seltmann et al. (2014)
Baishan	China, (Xinjiang)	Porphyry	Mo	Post-orogenic to intracontinental extensional environment	Granite porphyry	226.0 ± 229 Ma*	Disseminated, breccia	Mot, Cp, Py, Pyr	Q, Kf, Ch, Cb	Li et al. (2006), Zhu et al. (2013), Wang et al. (2015c), (2016c)

Table 6 (*continued*)

Deposit	Location	Deposit type	Commodity	Geodynamic setting	Major host rocks	Ore forming ages (Ma)	Ore textures	Major metal minerals	Alteration assemblage	References
Hadamengou-Liubagou	China, (Inner Mongolia)	Magmatic hydrothermal	Au, Mo	Mo: southward subduction of the Paleo-Asian Ocean beneath the NCC in Late Devonian; Au: post-collisional extension in Triassic	Gneiss	355–382 Ma* (Mo) 218–240 Ma (Au)	Veined, veinlet, disseminated, breccia	Py, Mt, Gn, Cp, Mot, Gl	Potassic (Kf-Q-Bi-Mt), phyllic (Q-Py), propylitic (Q-Ch-Ep-Py-Cb)	This study and references cited therein
Liushashan		Porphyry	Mo, Au	Syn-collision setting between the Siberian and north Tarim plate	Monzogranite, granodiorite	260 ± 10 Ma*	Veined, disseminated-veinlet, stockwork	Mot, Sch, Py, Cp	Q, Kf, Bi, Ch, Cb	Nie et al. (2002), Yang et al. (2013)
Chaganhua			Mo, Cu	Syn-collision to post-collision setting between the Siberian and NCC	Biotite granite	242.7 ± 3.5 Ma*	Stockwork, disseminated-veinlet, veined	Py, Mot, Mt, Cp, Gn	Q, Kf, Ser, Mus	Xi et al. (2010), Cai et al. (2011a), Liu et al. (2012)
Chagandeersi			Mo, Cu		Biotite granite	243.0 ± 2.2 Ma*	Stockwork	Py, Mot, Wo, Bm, Cp, Sph	Q, Kf, Ser, Mus	Xi et al. (2010), Cai et al. (2011b)
Laojiagou			Mo, Cu		Monzogranite porphyry	234.9 ± 3.1 Ma*	Disseminated, stockwork	Mot, Py, Cp	Q, Ser, Ch, Cb	Zeng et al. (2012)
Baituyingzi			Mo, Cu	Late stage of collision between Siberian and NCC	Monzogranite	248 ± 10 Ma*	Veinlet, stockwork, disseminated, breccia	Mot, Py, locally Cp	Potassic (Kf-Q-Hem), phyllic (Ser-Q-Mus-Ill), propylitic (Ch-Ep)	Sun et al. (2013)
Xishadegai			Mo	Post-collision regime	Porphyritic granite, porphyritic moyite	225.4±2.6 Ma*	Veined, stockwork, disseminated	Mot, Py, locally Cp	Kf, Q, Ser, Py, Kln	Zhang et al. (2011a, b), Zhang (2012), Sun (2016)
Xiaohulishan			Mo	Intraplate tectonic setting and stretching-extrusion structure	Granite	220.0 ± 2.2 Ma*	Disseminated, stockwork	Mot, Py, Sph, Gn	Q, Kf, Ser, Ep, Ch, Cb	Shen et al. (2010), Peng et al. (2010), Yang et al. (2013)
Kulitu		Mesothermal quartz vein	Mo, Cu	Syn-collision to post-collision setting between the Siberian and NCC	Monzogranite	245.0 ± 4.3 Ma*	Veined, stockwork, disseminated	Py, Mot, Cp, Bo	Q, Kf, Ser, Mus, Ill, Ch, Hem, Cb	Zeng et al. (2012), Sun et al. (2013)
Baimashi			Cu, Mo		Porphyritic granite	248.6 ± 6.7 Ma*	Veined, stockwork, disseminated	Cp, Bo, Mot, Py	Q, Kf, Bi, Hem, Ser, Ch, Ep, Ser, Kln, Cb	Zeng et al. (2012), Sun et al. (2013)

Ore and alteration mineral abbreviations: Ab = albite, Ars = arsenopyrite, Bi = biotite, Bm = bismuthine, Bo = bornite, Cal = calcite, Cb = carbonate, Ch = chlorite, Cp = chalcopyrite, Cha = chalcocite, Dg = digenite, Ep = epidote, Enr = enargite, Ill = illite, Gn = galena, Gold = Gl, Hem = Hematite, Kf = K-feldspar, Kln = kaolinite, Mt = magnetite, Mus = muscovite, Mot = molybdenite, Prh=prehnite, Py = pyrite, Pyr = pyrrhotite, Q = quartz, Ser=sericite, Sph = sphalerite, Snt = stibnite, Sh = scheelite, Tur = tourmaline, Td = tetrahedrite, Ten = Tennantite, Wo = wolframite.
*Mineralization ages are based on Re-Os isochron ages of molybdenite, geochronological data without * represent U-Pb ages of mineralized granitoids.

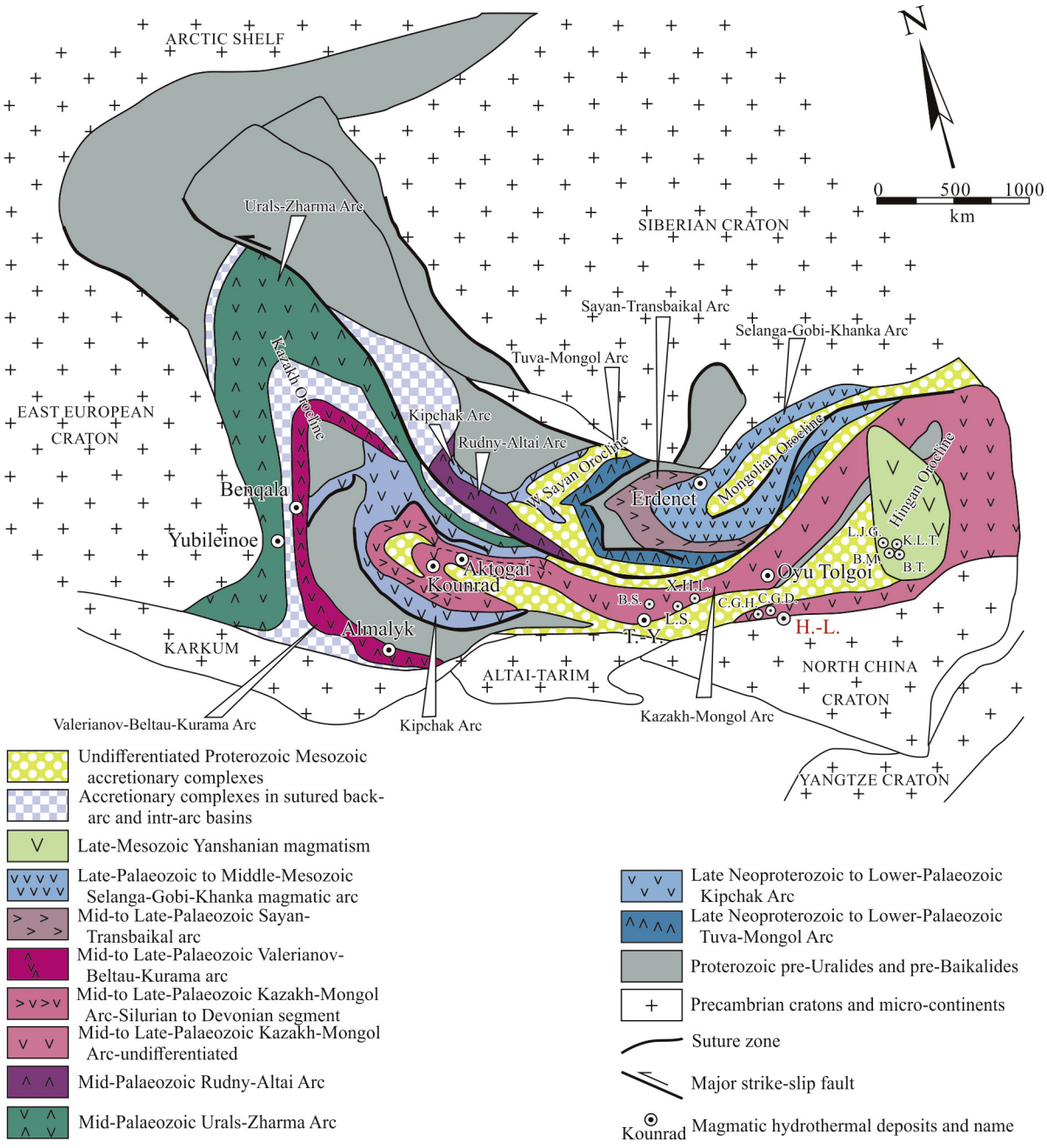

Fig. 14. Schematic map showing the distribution of major magmatic hydrothermal Cu, Au, Mo deposits and island-arcs of the Central Asia Metallogenic Domain (modified after Seltmann et al., 2014). Abbreviations of deposits in China is the same as Fig. 1.

2013). In the study area, the Xishadegai Mo deposit (~225 Ma) to the north of Hadamengou-Liubagou represents product of post-collision regime. The Au-Mo deposits are represented for Liushashan and Hadamengou-Liubagou (Table 6). As for the Liushashan Mo-Au deposit, Mo mineralization occurs at ~260 Ma (Nie et al., 2002), however, time of Au mineralization is unclear because of the lack of suitable minerals for isotopic dating. Bian (2015) infers that the Au mineralization overprinted on the earlier porphyry Mo mineralization based on deposit geology. In Hadamengou-Liubagou deposit, detailed paragenetic studies in this paper and the most reliable stepwise ^{40}Ar-^{39}Ar ages (218–240 Ma) on the Au mineralization imply that Au mineralization overprinted on the Devonian Mo mineralization, and formed in Triassic post-collisional setting.

Overall, Both Mo and Au ore veins at Hadamengou-Liubagou are structurally controlled, and temporally and spatially associated with contemporaneous granitic intrusives. They are not directly related to porphyry systems although some comparable alteration mineral assemblages existing, but, are products of the same large scale metallogenic evolution under subduction setting in Devonian and post-collisional extension environment in Triassic.

6. Conclusions

The Hadamengou-Liubagou Au-Mo deposit at the north margin of the NCC is a magmatic hydrothermal deposit hosted in the Archean amphibolite to granulite facies metamorphic rocks. The orebodies typically occur as a series of subparallel, fault-

controlled quartz veins and potassic-altered and silicified rocks. Hydrothermal mineral assemblages are divided into four stages, including K-feldspar-quartz-molybdenite stage (I), quartz-pyrite-epidote/chlorite stage (II), quartz-polymetallic sulfide-gold stage (III), and carbonate-sulfate-quartz stage (IV). Gold and molybdenum mineralization occurred mainly in stage III and stage I, respectively. Hydrogen and oxygen isotopes indicate that the ore-forming fluids were dominated by magmatic water with minor meteoric water. Sulfur and carbon isotopes suggest a magmatic origin. There exist two mineralizing events associated with magmatic activities in the study area. The Variscan event is related to the Mo mineralization at Hadamengou-Liubagou (382–355 Ma). The Indosinian event is suggested to be responsible for both the gold mineralization in the Hadamengou-Liubagou deposit (240–218 Ma) and the Mo mineralization at Xishadegai (~225 Ma). Two mineralizing events at Hadamengou-Liubagou Au-Mo are products of the same large scale metallogenic evolution under Devonian subduction setting and Triassic post-collisional extension environment.

Acknowledgements

We are grateful to geologists of the Second Gold Geological Party of CAPF, Dr. Lei Shibin from Gold Headquarters of CAPF, and Li Wei from Xinda Gold Mining Co. Ltd. of China for their great support and assistance. The manuscript has been significantly improved from constructive comments by Dr. Thierry Bineli Besti and Dr. Harald G. Dill. Insightful handling and valuable comments from editors is also greatly appreciated. The authors wish to thank Brian Rusk from Western Washington University for constructive discussions and his permission to conduct work in the SEM-EDS labratory. We also appreciate Sun Xuan, Charles Wandler, Ouyang Xin, and Bai Wei for their assistance. The research was funded by the National Natural Science Foundation of China (NSFC) under grants of 41302064, 41572062 and U1303292, the Specialized Research Fund for the Doctoral Program of Higher Education (SRFDP, 20130022120016), and the state scholarship fund provided by China Scholarship Council.

References

Abdulin, A.A., Bespaev, H.A., Daukeev, C.Zh., Miroshnichenko, L.A., Votsalevskiy, E.S., 1998, Copper deposits of Kazakhstan, Reference Book: Ministry of Ecology and Natural Resources of the Republic of Kazakhstan, Almaty, Kazakhstan, p. 1–141.

Baker, T., 2002. Emplacement depth and carbon dioxide-rich fluid inclusions in intrusion-related gold deposit. Econ. Geol. 97 (5), 1111–1117.

Bian, P., 2015. Discussion on ore genesis and metallogenic model of the Liushashan Mo-Au deposit, Inner Mongolia. Acta Mineral. Sin. S1, 268–269 (in Chinese).

Cai, M.H., Zhang, Z.G., Qu, W.J., Peng, Z.A., Zhang, S.Q., Xu, M., Chen, Y., Wang, X.B., 2011a. Geological characteristics and Re-Os dating of the Chaganhua molybdenum deposit in Urad Rear Banner, Western Inner Mongolia. Acta Geosci. Sin. 32, 64–68 (in Chinese with English abstract).

Cai, M.H., Peng, Z.A., Qu, W.J., He, Z.Y., Feng, G., Liu, S.Q., Xu, M., Chen, Y., 2011b. Geological characteristics and Re–Os dating of molybdenites in Chagandeersi molybdenum deposit, western Inner Mongolia. Mineral Deposits 30, 377–384 (in Chinese with English abstract).

Cao, H.H., Xu, W.L., Pei, F.P., Wang, Z.W., Wang, F., Wang, Z.J., 2013. Zircon U-Pb geochronology and petrogenesis of the late Paleozoic-early Mesozoic intrusive rocks in the eastern segment of the northern margin of the north China block. Lithos 170, 191–207.

Cao, M.J., Li, G.M., Qin, K.Z., Evans, N.J., Seitmuratova, E.Y., 2016. Assessing the magmatic affinity and petrogenesis of granitoids at the giant Aktogai porphyry Cu deposit. Central Kazakhstan 316, 614–668.

Chen, J.M., Liu, G., Li, C.C., 1996. Geology of greenstone-type gold deposits in the Wulashan-Daqingshan Mt, Inner Mongolia, Beijing. Geological Publishing House, 1–121 (in Chinese).

Chen, X., Seitmuratova, E., Wang, Z., Chen, Z., Han, S., Li, Y., Ye, B., Shi, W., 2014. Shrimp U-Pb and Ar–Ar geochronology of major porphyry and skarn Cu deposits in the Balkhash Metallogenic Belt, Central Asia, and geological implications. J. Asian Earth Sci. 79, 723–740.

Chen, Y.J., Ni, P., Fan, H.R., Pirajno, F., Lai, Y., Su, W.C., Zhang, H., 2007. Diagnostic fluid inclusions of different types hydrothermal gold deposits. Acta Petrol. Sin. 23, 2085–2108 (in Chinese with English abstract).

Chen, Y.J., Li, N., 2009. Nature of ore-fluids of intracontinental intrusion-related hypothermal deposits and its difference from those in island arcs. Acta Petrol. Sin. 25, 2477–2508 (in Chinese with English abstract).

Chen, Y.J., Pirajno, F., Li, N., Guo, D.S., Lai, Y., 2009. Isotope systematics and fluid inclusion studies of the Qiyugou breccia pipe-hosted gold deposit, Qinling Orogen, Henan province, China: implications for ore genesis. Ore Geol. Rev. 35, 245–261.

Clayton, R.N., Mayeda, T.K., 1963. The use of bromine pentafluoride in the extraction of oxygen from oxides and silicates for isotopic analysis. Geochim. Cosmochim. Acta 27, 43–52.

Clayton, R.N., O'Neil, J.R., Mayeda, T.K., 1972. Oxygen isotope exchange between quartz and water. J. Geophys. Res. 77, 3057–3067.

Cooke, D.R., McPhail, D.C., 2001. Epithermal Au-Ag-Te mineralization, Acupan, Baguio district, Philippines: numerical simulations of mineral deposition. Econ. Geol. 96, 109–131.

Dill, H.G., 2010. The "chessboard" classification scheme of mineral deposits: mineralogy and geology from aluminum to zirconium. Earth Sci. Rev. 100 (1–4), 1–420.

Du, A.D., Wu, S.Q., Sun, D.Z., Wang, S.X., Qu, W.J., Markey, R., Stain, H., Morgan, J., Malinovskiy, D., 2004. Preparation and certification of Re-Os dating reference materials molybdenite HLP and JDC. Geostand. Geoanal. Res. 28, 41–52.

Éric, M., Khadija, N., Yannick, B., Claire, R., Gilles, R., Jean-Jacques, P., Ross, S., Michel, J., 2015. Late-Hercynian intrusion-related gold deposits: an integrated model on the Tighza polymetallic district, central Morocco. J. Afr. Earth Sc. 107, 65–88.

Faure, G., Mensing, T.M., 2005. Isotopes: Principles and Applications. John Wiley & Sons Inc.

Fairmaid, A.M., Kendrick, M.A., Phillips, D., Fu, B., 2011. The origin and evolution of mineralizing fluids in a sediment-hosted orogenic-gold deposit, Ballarat East, Southeastern Australia. Econ. Geol. 106, 653–666.

Friedman, I., O'Neil, J.R., Fleischer, M., 1977. Compilation of stable isotope fractionation factors of geochemical interest. U. S. Geological Survey Professional Paper, KK1-12.

Gan, S.F., Qiu, Y.M., Yang, H.Y., Van Reenen, D.D., 1994. The Hadamengou mine: a typical gold deposit in the Archean granulite facies terrane of the North China craton. Int. Geol. Rev. 36, 850–866.

Gold Headquarter of Chinese Armed Police Force (GHCAPF), 1995. Geology of the Hadamengou pegmatitic gold deposit occurring in Inner Mongolia Autonomous region. Beijing, Seismological Press, 1–227 (in Chinese with English abstract).

Gold Headquarter of Chinese Armed Police Force (GHCAPF), No.2, 2011, 2011. Gold prospecting report in the Hadamengou and peripheral area. Inner Mongolia, Hohhot (in Chinese).

Goldfarb, R.J., Marsh, E.E., Bradley, D., Johnson, C., Miller, M.L., Ebert, S.W., Petsel, S. A., Miller, L.D., Mcclelland, W., 2004. The Late Cretaceous Donlin Creek Gold Deposit, Southwestern Alaska: Controls on Epizonal Ore Formation. Econ. Geol. 99 (4), 643–671.

Groves, D.I., Goldfarb, R.J., Gebre-Mariam, M., Hagemann, S.G., Robert, F., 1998. Orogenic gold deposits: A proposed classification in the context of their crustal distribution and relationship to other gold deposit types. Ore Geol. Rev. 13, 7–27.

Groves, D.I., Condie, K.C., Goldfarb, R.J., Hronsky, J.M.A., Vielreicher, R.M., 2005. Secular changes in global tectonic processes and their influence on the temporal distribution of gold-bearing mineral deposits. Econ. Geol. 100, 203–244.

Groves, D.I., Bierlein, F.P., 2007. Geodynamic settings of mineral deposit system. J. Geol. Soc. 164, 19–30.

Gu, F.H., Zhang, Y.M., Liu, R.P., Zheng, L., Sun, X., 2015. Magma mixing and mingling of the Shadegai granite in Inner Mongolia: Evidence from petrography, mineral chemistry and geochronology. Acta Petrol. Sin. in press (in Chinese with English abstract).

Guan, L.X., Li, J.M., Cai, S.B., 1992. Study on geological characteristics of gold deposits and ore prospecting targets in Wulashan-Dingshan area, Inner Mongolia. Gold geological institute of gold headquarters of China, Langfang (in Chinese).

Guo, Y.T., 1992. The minerogenetic geology of Hadamengou type gold deposits in Wulashan, Inner Mongolia. J. Precious Metal Geol. Z1, 191–195 (in Chinese with English abstract).

Han, C.M., Xiao, W.J., Zhao, G.C., Mao, J.W., 2006. Geological characteristics and genesis of the Tuwu porphyry copper deposit, Hami, Xinjiang, central Asia. Ore Geol. Rev. 28, 308–328.

Hart, C.J.R., Goldfarb, R.J., Qiu, Y.M., Snee, L., Miller, L.D., Miller, M.L., 2002. Gold deposits of the northern margin of the North China Craton: multiple late Paleozoic-Mesozoic mineralizing events. Miner. Deposita 37. 326-251.

Hoefs, J., 2008. Stable Isotope Geochemistry. Spriger-Verlag, Berlin, pp. 103–136.

Hou, W.R., Nie, F.J., Du, A.D., Liu, Y.F., Yun, F., Zhang, K., Liu, Y., Bian, H.Y., Liu, H.L., 2011. Isotopic evidence for determining the Devonian gold and molybdenum mineralization in the Hadamengou area, Baotou, Inner Mongolia. Geol. Rev. 57, 583–590 (in Chinese with English abstract).

Hou, W.R., 2011. Comparison study on the Hadamengou gold deposit and Jinchagngouliang gold deposit, Inner Mongolia. Beijing, Graduate School of Chinese Academy of Geological Sciences, 1–213 (Doctoral dissertation, in Chinese with English abstract).

Jiang, S.H., Nie, F.J., Su, Y.J., Bai, D.M., Liu, Y.F., 2010. Geochronology and origin of the Erdenet superlarge Cu-Mo deposit in Mongolia. Acta Geosci. Sin. 31, 289–306 (in Chinese with English abstract).

Kirwin, D.J., Forster, C.N., Kavalieris, I., Crane, D., Orssich, C., Panther, C., Garamjav, D., Munkhbat, T.O., Niislelkhuu, G., 2005. The Oyu Tolgoi copper-gold porphyry deposits, South Gobi, Mongolia. In: Seltmann, R., Gerel, O., Kirwin, D.J. (Eds.),

Geodynamics and Metallogeny of Mongolia with a Special Emphasis on Copper and Gold Deposits. International Association on the Genesis of Ore Deposits, London, pp. 155–168.
Klemm, L.M., Pettke, T., Heinrich, C.A., 2008. Fluid and source magma evolution of the Questa porphyry Mo deposit, New Mexico, USA. Miner. Deposita 43, 533–552.
Kontak, D.J., Kerrich, R., 1997. An isotopic (C, O, Sr) study of vein gold deposits in the Meguma terrane, Nova Scotia: Implication for source reservoirs. Econ. Geol. Bull. Soc. Econ. Geol. 92, 161–180.
Kudryavtsev, Y.K., 1996. The Cu-Mo deposits of central Kazakhstan. In: Shatov, V., Seltmann, R., Kremenetsky, A., Lehmann, B., Popov, V., Ermolov, P. (Eds.), Granite-related ore deposits of central Kazakhstan and adjacent area. Glagol Publishing House, St. Petersburg, pp. 119–144.
Lang, D.Y., 1990. Geological characteristics and ore-forming controls of Wulashan gold deposit, Inner Mongolia. Geol. Inner Mongolia 2, 30–40 (in Chinese).
Lang, D.Y., Li, W., 1998. Study gold ore belt sulfur isotopic characteristics in Wulashan, Inner Mongolia. Geol. Inner Mongolia 86, 24–34 (in Chinese with English abstract).
Lang, J.R., Baker, T., 2001. Intrusion-related gold systems: the present level of understanding. Miner. Deposita 36, 477–489.
Li, C.M., Zhang, C.H., Cope, T.D., Lin, Y., 2016. Out-of-sequence thrusting in polycyclic thrust belts: an example from the Mesozoic Yanshan belt, North China Craton. Tectonics 35, 2082–2116.
Li, D.P., Chen, Y.L., Chen, L.M., Wang, Z., Liu, J.B., 2009. Zircon LAICPMS study and petrogenesis simulation of Dahuabei pluton in the Wulashan area, Inner Mongolia. Prog. Nat. Sci. 19, 1727–1737.
Li, G.M., Cao, M.J., Qin, K.Z., Hollings, P., Evans, N.J., Seitmuratova, E.Y., 2016. Petrogenesis of ore-forming and pre/post-ore granitoids from the Kounrad, Borly and Sayak porphyry/skarn Cu deposits, Central Kazakhstan. Gondwana Res. 37, 408–425.
Li, H.Q., Chen, F.W., Li, J.Y., Qu, W.J., Wang, D.H., Deng, G., Mei, Y.P., 2006. Age of mineralization and host rocks in the Baishan rhenium-molybdenum district, East Tianshan, Xinjiang, China: Revisited. Geol. Bull. China 25, 916–922 (in Chinese with English abstract).
Li, J.Y., 1998. Some new ideas on tectonics of NE China and its neighboring areas. Geol. Rev. 44, 339–347 (in Chinese with English abstract).
Li, J.Y., 2006. Permian geodynamic setting of Northeast China and adjacent regions: closure of the Paleo-Asian Ocean and subduction of the Paleo-Pacific Plate. J. Asian Earth Sci. 26, 207–224.
Liu, J.M., Liu, J.J., 1997. Basin fluid genetic model of sediment-hosted micro-disseminated gold deposits in the gold-triangle area between Guizhou, Guangxi and Yunnan. Acta Mineral. Sin. 17, 448–456 (in Chinese with English abstract).
Liu, Y.F., Nie, F.J., Jiang, S.H., Xi, Z., Zhang, Z.G., Xiao, W., Zhang, K., Liu, Y., 2012. Ore-forming granites from Chaganhua molybdenum deposit, Central Inner Mongolia, China: geochemistry, geochronology and petrogenesis. Acta Petrol. Sin. 28, 409–420 (in Chinese with English abstract).
Ludwig, K.R., 2004. Isoplot/Ex, version 3.0: A Geochronological Toolkit for Microsoft Excel. Berkeley Geochronology Center, Berkeley CA.
Melfos, V., Voudouris, P., 2016. Fluid evolution in Tertiary magmatic-hydrothermal ore systems at the Rhodope metallogenic province, NE Greece. A review. Geol. Croat. 69, 157–167.
Meng, W., Chen, X.W., Li, M.W., 2002. Study on metallogenic epoch and metallogenic stages of the Hadamengou gold deposit, Inner Mongolia. Gold Geol. 8, 13–17 (in Chinese with English abstract).
Miao, L.C., Qiu, Y.M., Guan, K., McNaughton, N., Qiu, Y.S., Luo, Z.K., Groves, D., 2000. Shrimp chronological study of the granitoids and mineralization in the Hadamengou gold deposit, Inner Mongolia. Mineral Deposits 19, 182–190 (in Chinese with English abstract).
Mutschler, F.E., Ludington, S. and Bookstrom, A.A., 2000. Giant porphyry-related metal camps of the world—a database; U.S. Geological Survey Open-File Report 99-556, Online Version 1.0, http://geopubs.wr.usgs.gov/open-file/of99-556/world_ppy.xls.
Müller, D., Groves, D.I., 1997. Potassic Igneous Rocks and Associated Gold-Copper Mineralization. Springer-Verlag, Berlin Heidelberg. 1998.
Nie, F.J., 1995. Nd-Sr-Pb isotope study of Wulashan quartz-feldspar vein-type gold deposits in Inner Mongolia. Institute of Mineral Resources Chinese Academy of Geological Sciences, Beijing, pp. 1–56 (in Chinese).
Nie, F.J., Bjorlykke, A., 1994. Lead and sulfur isotope studies of the Wulashan quartz-K feldspar and quartz vein gold deposit, southwestern Inner Mongolia, People's Republic of China. Econ. Geol. 89, 1289–1305.
Nie, F.J., Jiang, S.H., Zhao, X.M., Bai, D.M., Liu, Y., Zhao, Y.M., Wang, X.L., Su, X.X., 2002. Geological features and metallogenic type of the Liushashan gold (molybdenum) deposit in Ejin Qi (Prefecture), Western Inner Mongolia. Geology-Geochem. 30, 1–7 (in Chinese with English abstract).
Nie, F.J., Jiang, S.H., Liu, Y., Hu, P., 2005. Re-discussions on the time limitation of gold mineralization occurring within the Hadamengou deposit, south-central Inner Mongolia autonomous region. Acta Petrol. Sin. 21, 1719–1728 (in Chinese with English abstract).
Nie, F.J., Zhang, K., Liu, Y.F., Jiang, S.H., Liu, Y., Liu, Y., 2011. Indosinian magmatic activity and molybdenum, gold mineralization along the northern margin of North China Craton and adjacent area. J. Jilin Univ. (Earth Sci. Ed.) 41, 1651–1666 (in Chinese with English abstract).
Nie, F.J., 1997. Type and distribution of gold deposits along the northern margin of the North China Craton, People's Republic of China. Int. Geol. Rev. 39, 151–180.
Ohmoto, H., 1972. Systematics of sulfur and carbon isotopes in hydrothermal ore deposits. Econ. Geol. 67, 551–578.
Peng, Z.A., Li, H.H., Qu, W.J., Zhang, S.Q., Ding, H.J., Chen, X.R., Zhang, B., Zhang, Y.Z., Xu, M., Cai, M.H., 2010. Molybdenite Re-Os age of Xiaohulishan molybdenum deposit in Beishan area, Inner Mongolia. Mineral Deposits 29, 510–516 (in Chinesewith English abstract).
Perello, J., Cox, D., Garamjav, D., Sanjdorj, S., Diakov, S., Schissel, D., Munkhbat, T.O., Oyun, G., Oyun, G., 2001. Oyu Tolgoi, Mongolia: Siluro-Devonian Porphyry Cu-Au-(Mo) and High-Sulfidation Cu Mineralization with a Cretaceous Chalcocite Blanket. Econ. Geol. 96, 1407–1428.
Ridley, J.R., Diamond, L.W., 2000. Fluid chemistry of orogenic lode gold deposits and implications for genetic models. Gold 2000, 141–162.
Rye, R.O., Ohmoto, H., 1974. Sulfur and carbon isotopes and ore genesis: a review. Econ. Geol. 69, 826–842.
Rui, Z.Y., Zhang, L.S., Wang, Y.T., Liu, Y.L., 2002, Discussion on metallogenic epoch of Tuwu and Yandong porphyry copper deposits in East Tianshan Mountains, Xinjiang: Mineral Deposits, 21, pp. 16–22 (in Chinese with English abstract).
Saunders, C.M., Tuach, J., 1991. Potassic and sodic alteration accompanying gold mineralization in the Rattling Brook Deposit, western White Bay, Newfoundland Appalachians. Econ. Geol. 86, 555–569.
Seltmann, R., Shatov, V., Yakubchuk, A., 2004, Mineral deposits database and thematic maps of Central Asia, scale 1.5 million: ArcView 3.2 and MapInfo 6.0 (7.0) GIS Packages, Explanatory Notes, CERCAMS, Natural History Museum, London, UK, p. 117.
Seltmann, R., Porter, T.M., 2005. The porphyry Cu-Au/Mo deposits of Central Eurasia: 1. Tectonic, geologic, and metallogenic setting and significant deposits. In: Porter T.M. (Ed.). Super Porphyry Copper and Gold Deposit: A Global Perspective. Adelaide: PGC Publishing, vol. 2, pp. 467–512.
Seltmann, R., Porter, T.M., Pirajno, F., 2014. Geodynamics and metallogeny of the central Eurasian porphyry and related epithermal mineral systems: a review. J. Asian Earth Sci. 79, 810–841.
Shen, C.L., Zhang, M., Yu, X.Q., Chen, W.G., Gao, W.Y., Zhou, W.C., 2010. New progresses in exploration of molybdenum deposits and analysis of mineralization prospect in Inner Mongolia. Geol. Explor. 46, 561–575 (in Chinese with English abstract).
Shen, P., Pan, H.D., Zhou, T.F., Wang, J.B., 2014a. Petrography, geochemistry and geochronology of the host porphyries and associated alteration at the Tuwu Cu deposit, NW China: a case for increased depositional efficiency by reaction with mafic hostrock? Miner. Deposita 49, 709–731.
Shen, P., Pan, H., Dong, L., 2014b. Yandong porphyry Cu deposit, Xinjiang, China—geology, geochemistry and SIMS U-Pb zircon geochronology of host porphyries and associated alteration and mineralization. J. Asian Earth Sci. 80, 197–217.
Shen, P., Hattori, K., Pan, H., Jackson, S., Seitmuratova, E., 2015. Oxidation Condition and Metal Fertility of Granitic Magmas: Zircon Trace-Element Data from Porphyry Cu Deposits in the Central Asian Orogenic Belt. Econ. Geol. 110, 1861–1878.
Shen, Y., Gu, X.X., Zhang, Y.M., Liu, L., 2010. Fluid inclusion study of Liubagou gold deposit in Inner Mongolia. Uranium Geol. 26, 158–165 (in Chinese with English abstract).
Shi, G.R., 2006. Marine Permian in East and NE Asia: biostratigraphy, palaeobiogeography and palaeogeographical implications. J. Asian Earth Sci. 26, 175–206.
Sillitoe, R.H., Thompson, J.F.H., 1998. Intrusion-related vein gold deposits: types, tectono-magmatic settings and difficulties of distinction from orogenic gold deposits. Resour. Geol. 48, 237–250.
Sillitoe, R.H., 2010. Porphyry copper systems. Econ. Geol. 105, 3–41.
Sun, X., 2016. Geological, geochemistry charecteristics and genesis of Xishadegai porphyry type ore deposit, Inner Mongolia. Beijing, China University of Geosciences, pp. 1–79 (Master dissertation, in Chinese with English abstract).
Sun, Y., Liu, J.M., Zeng, Q.D., Chu, S.X., Zhou, L.L., Wu, G.B., Gao, Y.Y., Shen, W.J., 2013. Geological characteristics and molybdenite Re-Os ages of the Baituyingzi Mo–Cu field, eastern Inner Mongolia and their geological implications. Acta Petrol. Sin. 29, 242–254 (in Chinese with English abstract).
Taylor, H.P., 1974. The application of oxygen and hydrogen isotope studies to problems of hydrothermal alteration and ore deposition. Econ. Geol. 69 (6), 843–883.
Tombros, S., Seymour, K.S., Williams-Jones, A.E., 2010. Controls on Tellurium in Base, Precious, and Telluride Minerals in the Panormos Bay Ag-Au-Te Deposits, Tinos Island, Cyclades, Greece. Econ. Geol. 105, 1097–1111.
Watanabe, Y., Stein, H.J., 2000. Re-Os ages for the Erdenet and Tsagaan Suvarga porphyry Cu-Mo deposits, Mongolia, and tectonic implications. Econ. Geol. 95, 1537–1542.
Windley, B.F., Alexeiev, D., Xiao, W., Kröner, A., Badarch, G., 2007. Tectonic models for the accretion of the Central Asian orogenic belt. J. Geol. Soc. 164, 31–47.
Wu, F.Y., Sun, D.Y., Li, H.M., Jahn, B.M., Wilde, S., 2002. A-type granites in northeastern China: age and geochemical constraints on their petrogenesis. Chem. Geol. 187, 143–173.
Wang, Y.H., Xue, C.J., Liu, J.J., Wang, J.P., Yang, J.T., Zhang, F.F., Zhao, Z.N., Zhao, Y.J., Liu, B., 2015a. Early Carboniferous adakitic rocks in the area of the Tuwu deposit, eastern Tianshan, NW China: Slab melting and implications for porphyry copper mineralization. J. Asian Earth Sci. 103, 332–349.
Wang, Y.H., Xue, C.J., Wang, J.P., Peng, R.M., Yang, J.T., Zhang, F.F., Zhao, Z.N., Zhao, Y.J., 2015b. Petrogenesis of magmatism in the Yandong region of Eastern Tianshan, Xinjiang: Geochemical, geochronological and Hf isotope Constraints. Int. Geol. Rev. 57, 1130–1151.
Wang, Y.H., Zhang, F.F., Liu, J.J., Xue, C.J., Wang, J.P., Liu, B., Lu, W.W., 2015c. Petrogenesis of granites in Baishan molybdenum deposit, eastern Tianshan,

Xinjiang: Zircon U-Pb geochronology, geochemistry, and Hf isotope constraints. Acta Petrol. Sin. 31, 1962–1976 (in Chinese with English Abstract).
Wang, Y.H., Zhang, F.F., Liu, J.J., Que, C.Y., 2016a. Genesis of the Fuxing porphyry Cu deposit in Eastern Tianshan, China: Evidence from fluid inclusions and C-H–O–S–Pb isotope systematics. Ore Geol. Rev. 79, 46–61.
Wang, Y.H., Zhang, F.F., Liu, J.J., 2016b. The genesis of the ores and intrusions at the Yuhai Cu–Mo deposit in eastern Tianshan, NW China: constraints from geology, geochronology, geochemistry, and Hf isotope systematics. Ore Geol. Rev. 77, 312–331.
Wang, Y.H., Xue, C.J., Liu, J.J., Zhang, F.F., 2016c. Geological, geochronological, geochemical, and Sr–Nd–O–Hf isotopic constraints on origins of intrusions associated with the Baishan porphyry Mo deposit in eastern Tianshan. NW China. Miner. Deposita 51, 953–969.
Wang, Y.J., Fan, Z.Y., 1997. Discovery of Permian radiolariansin ophiolite belt on northern side of Xar Moron River, Nei Monggol and its geological significance. Acta Palaeontol. Sin. 36, 59–69 (in Chinese with English Abstract).
Wang, C.W., Jin, W., Zhang, X.Z., Ma, Z.H., Chi, X.G., Liu, Y.J., Li, N., 2008. New understanding of the Late Paleozoic tectonics in northeastern China and adjcent areas. J. Stratigr. 32, 119–136 (in Chinese with English abstract).
Wang, W.L., Guo, S.Z., 2012. The evolution and transformation of Paleo-Asia and Paleo-Pacific tectonic domain of northeast China. Geol. Resour. 21, 27–34 (in Chinese with English abstract).
Wang, L., Wang, G.H., Lei, S.B., Wei, G.F., Jia, L.Q., Chang, C.X., 2014. Re-Os dating of molybdenite from Hadamengou gold ore field in Inner Mongolia and its geological significance. Acta Geol. Sin. (English Ed.) 88, 1017–1018.
Wang, L., 2016. Tectono-magmatic process and metallogenesis of Hadamengou gold ore field, Inner Mongolia. Beijing, China University of Geosciences, pp. 1–259 (Doctoral dissertation, in Chinese with English abstract).
Wainwright, A.J., Tosdal, R.M., Wooden, J.L., Mazdab, F.K., Friedman, R.M., 2011. U-Pb (zircon) and geochemical constraints on the age, origin, and evolution of Paleozoic arc magmas in the Oyu Tolgoi porphyry Cu–Au district, southern Mongolia. Gondwana Res. 19, 764–787.
Xi, Z., Zhang, Z.G., Jia, L.J., Gou, X.J., Sun, Q.R., Hou, W.R., 2010. The discovery of the Manitu-Chaganhua large-size Mo–Bi–W mineralized district, Inner Mongolia, and its geological significance. Acta Geosci. Sin. 31, 466–468 (in Chinese with English abstract).
Xiao, W., Windley, B.F., Hao, J., 2003. Accretion leading to collision and the Permian Solonker suture, Inner Mongolia, China: termination of the central Asian orogenic belt. Tectonics 22, 1069. http://dx.doi.org/10.1029/2002TC001484.
Xie, Y., 2011. Research on the metallogenic source and genesis of Hadamengou Au deposit in Inner Mongolia, Shijiazhuang. Shijiazhuang University of Economics, 26–38 (in Chinese with English abstract).
Xue, C.J., Zhao, X.B., Mo, X.X., 2016. Problem on porphyry Cu-Au metallogenic environment in Central Asian: an overview. Acta Petrol Sin. 32, 1249–1261 (in Chinese with English abstract).
Yan, G.H., Mou, B.L., Xu, B.L., He, G.Q., Tan, L.K., Zhao, H., He, Z.F., 2000. Geochronology and Sr-Nd-Pb isotope characteristics of the Triassic alkaline intrusions in Yanliao-Yinshan district. Sci. China Ser. D: Earth Sci., 30, 383–387 (in Chinese).
Yang, J.H., Wu, F.Y., Wilde, S.A., 2003. A review of the geodynamic setting of large-scale Late Mesozoic gold mineralization in the North China Craton: an association with lithospheric thinning. Ore Geol. Rev. 23, 125–152.
Yang, Y.Q., Zhao, J.H., Meng, G.X., Yan, J.Y., Lv, B., Wang, S.G., Jia, L.L., Han, J.G., 2013. Rock-forming and ore-forming ages as well as formation environments of porphyry molybdenum deposits in Beishan area, Inner Mongolia. Acta Geosci. Sin. 34, 401–412 (in Chinese with English abstract).
Zeng, Q.D., Liu, J.M., Chu, S.X., Wang, Y.B., Sun, Y., Duan, X.X., Zhou, L.L., 2012. Mesozoic molybdenum deposits in the East Xingmeng orogenic belt, northeast China: characteristics and tectonic setting. Int. Geol. Rev. 54, 1–27.
Zeng, Q.D., Qin, K.Z., Liu, J.M., Li, G.M., Zhai, M.G., Chu, S.X., Guo, Y.P., 2015. Porphyry molybdenum deposits in the Tianshan-Xingmeng orogenic belt, northern China. Int. J. Earth Sci. 104, 991–1023.
Zhang, C.H., Wu, G.G., Xu, D.B., Wang, G.H., Sun, W.H., 2004. Mesozoic tectonic framework and evolution in the central segment of the intraplate Yanshan orogenic belt. Geol. Bull. China 23, 864–875 (in Chinese with English abstract).
Zhang, H.T., So, C.S., Yun, S.T., 1999. Regional geologic setting and metallogenesis of central Inner Mongolia, China: guides for exploration of mesothermal gold deposits. Ore Geol. Rev. 14, 129–146.
Zhang, L.C., Wu H.Y., Xiang P., Zhang X.J., Chen Z.G., Wan B., 2010. Ore-forming processes and mineralization of complex tectonic system during the Mesozoic: A case from Xilamulun Cu-Mo metallogenic belt. Acta Petrol Sin, 26, 1351–1362 (in Chinese with English abstract).
Zhang, L.G., 1985. The application of the stable isotope to geology. Xi'an, Shanxi Science and Technology Publishing House, 152–186 (in Chinese with English abstract).
Zhang, X.H., Zhai, M.G., 2010. Magmatism and its metallogenetic effects during the Paleozoic continental crustal construction in northern North China: An overview. Acta Petrol. Sin. 26, 1329–1341 (in Chinese with English abstract).
Zhang, Y.M., Gu, X.X., Dong, S.Y., Cheng, W.B., Huang, Z.Q., Li, F.L., Yang, W.L., 2011a. Zircon U-Pb and molybdenite Re-Os dating for the Xishadegai molybdenum deposit in Inner Mongolia and its geological significance. J. Mineral. Petrol. 31, 33–41 (in Chinese with English abstract).
Zhang, Y.M., Gu, X.X., Cheng, W.B., Dong, S.Y., Huang, Z.Q., Li, F.L., Yang, W.L., 2011b. ^{40}Ar-^{39}Ar dating and lead isotopes of Liubagou gold deposit, Inner Mongolia. J. Jilin Univ. (Earth Sci. Ed.) 41, 1407–1422 (in Chinese with English abstract).
Zhang, Y.M., 2012. Metallogenesis, Ore-controlling factors and prospecting direction of the Liubagou-Hadamengou gold Deposit, Inner Mongolia. Beijing, China University of Geosciences (Beijing), pp. 1–254 (in Chinese with English abstract).
Zhu, Z.M., Xiong, X.L., Chu, F.Y., Wu, Y.H., 2013. Geochemistry and petrogenesis of core samples from Baishan molybdenum deposit, East Tianshan Mountains, Xinjiang. Acta Petrol. Sin. 29, 167–177 (in Chinese with English abstract).
Zou, T.R., Xu, J., Xia, F.R., 1998. Ore genesis of the Wulashan gold deposit, Inner Mongolia. Mineral Deposits, 17(Z), 373–376. (in Chinese).